



HAL
open science

Therapeutic inhibition of keratinocyte TRPV3 sensory channel by local anesthetic dyclonine

Qiang Liu, Jin Wang, Xin Wei, Juan Hu, Conghui Ping, Yue Gao, Chang Xie, Peiyu Wang, Peng Cao, Zhengyu Cao, et al.

► **To cite this version:**

Qiang Liu, Jin Wang, Xin Wei, Juan Hu, Conghui Ping, et al.. Therapeutic inhibition of keratinocyte TRPV3 sensory channel by local anesthetic dyclonine. eLife, 2021, 10, pp.e68128. 10.7554/eLife.68128 . hal-03204408

HAL Id: hal-03204408

<https://hal.sorbonne-universite.fr/hal-03204408v1>

Submitted on 21 Apr 2021

HAL is a multi-disciplinary open access archive for the deposit and dissemination of scientific research documents, whether they are published or not. The documents may come from teaching and research institutions in France or abroad, or from public or private research centers.

L'archive ouverte pluridisciplinaire **HAL**, est destinée au dépôt et à la diffusion de documents scientifiques de niveau recherche, publiés ou non, émanant des établissements d'enseignement et de recherche français ou étrangers, des laboratoires publics ou privés.

1 **Therapeutic inhibition of keratinocyte TRPV3 sensory**
2 **channel by local anesthetic dyclonine**

3 Qiang Liu^{1,6}, Jin Wang^{2,6}, Xin Wei¹, Juan Hu¹, Conghui Ping¹, Yue Gao¹,
4 Chang Xie¹, Peiyu Wang¹, Peng Cao³, Zhengyu Cao⁴, Ye Yu², Dongdong Li⁵,
5 Jing Yao¹✉

6 ¹ State Key Laboratory of Virology, Hubei Key Laboratory of Cell Homeostasis,
7 College of Life Sciences, Frontier Science Center for Immunology and
8 Metabolism, Wuhan University, Wuhan, Hubei 430072, China

9 ² School of Basic Medicine and Clinical Pharmacy, China Pharmaceutical
10 University, Nanjing, Jiangsu 211198, China

11 ³ Hospital of Integrated Traditional Chinese and Western Medicine, Nanjing
12 University of Chinese Medicine, Nanjing 210023

13 ⁴ State Key Laboratory of Natural Medicines and Jiangsu Provincial Key
14 Laboratory for TCM Evaluation and Translational Development, School of
15 Traditional Chinese Pharmacy, China Pharmaceutical University, Nanjing
16 Jiangsu 211198, China

17 ⁵ Sorbonne Université, Institute of Biology Paris Seine, Neuroscience Paris
18 Seine, CNRS UMR8246, INSERM U1130, Paris 75005, France

19 ⁶ These authors contributed equally to this work.

20

21 **Running title:** Inhibition of TRPV3 channels by dyclonine

22 **Keywords:** TRPV3, Dyclonine, Cell death, Pruritus, Skin inflammation

23 ☒ Address correspondence to:

24 Dr. Jing Yao

25 State Key Laboratory of Virology,

26 Hubei Key Laboratory of Cell Homeostasis,

27 College of Life Sciences,

28 Frontier Science Center for Immunology and Metabolism,

29 Wuhan University,

30 Wuhan, Hubei 430072, China

31 Phone: 86-27-68752148

32 Email: jyao@whu.edu.cn

33

34 **Abstract**

35 The multimodal sensory channel transient receptor potential vanilloid-3 (TRPV3) is
36 expressed in epidermal keratinocytes and implicated in chronic pruritus, allergy, and
37 inflammation-related skin disorders. Gain-of-function mutations of TRPV3 cause hair
38 growth disorders in mice and Olmsted Syndrome in human. Nevertheless, whether
39 and how TRPV3 could be therapeutically targeted remains to be elucidated. We here
40 report that mouse and human TRPV3 channel is targeted by the clinical medication
41 dyclonine that exerts a potent inhibitory effect. Accordingly, dyclonine rescued cell
42 death caused by gain-of-function TRPV3 mutations and suppressed pruritus
43 symptoms in vivo in mouse model. At the single-channel level, dyclonine inhibited
44 TRPV3 open probability but not the unitary conductance. By molecular simulations
45 and mutagenesis, we further uncovered key residues in TRPV3 pore region that could
46 toggle the inhibitory efficiency of dyclonine. The functional and mechanistic insights
47 obtained on dyclonine-TRPV3 interaction will help to conceive updated therapeutics
48 for skin inflammation.

49 **Introduction**

50 Transient receptor potential (TRP) channels belong to a family of calcium-permeable
51 and nonselective cation channels, essential for body sensory processing and local
52 inflammatory development (Clapham, 2003). As a polymodal cellular sensor, TRPV3
53 channel is abundantly expressed in skin keratinocytes (Chung, Lee, Mizuno, Suzuki,
54 & Caterina, 2004c; Peier et al., 2002; Xu et al., 2002) and in cells surrounding the hair
55 follicles (Cheng et al., 2010). TRPV3 integrates a wide spectrum of physical and
56 chemical stimuli (Luo & Hu, 2014). TRPV3 is sensitive to innocuous temperatures
57 above 30-33 °C and exhibits an increased response at noxious temperature (Chung,
58 Guler, & Caterina, 2005; Xu et al., 2002). Natural plant products such as camphor
59 (Moqrich et al., 2005), carvacrol, eugenol, thymol (Xu, Delling, Jun, & Clapham,
60 2006), and the pharmacological compound 2-aminoethoxydiphenyl borate (2-APB)
61 (Chung, Lee, Mizuno, Suzuki, & Caterina, 2004b; Colton & Zhu, 2007) also activate
62 TRPV3. In addition, TRPV3 is directly activated by acidic pH from cytoplasmic side
63 (Gao et al., 2016).

64 Mounting evidence implicates TRPV3 channel in cutaneous sensation including
65 thermal sensation (Chung et al., 2004c), nociception (S. M. Huang et al., 2008), and
66 itch (Yamamoto-Kasai et al., 2012). They also participate in the maintenance of skin
67 barrier, hair growth (Cheng et al., 2010) and wound healing (Aijima et al., 2015;
68 Yamada et al., 2010). Recently, the dysfunction of TRPV3 channels has come to the
69 fore as a key regulator of physio- and pathological responses of skin (Ho & Lee,

70 2015). In rodents, the Gly573Ser substitution in TRPV3 renders the channel
71 spontaneously active and caused a hairless phenotype in DS-Nh mice and
72 WBN/Kob-Ht rats (Asakawa et al., 2006). DS-Nh mice also develop severe scratching
73 behavior and pruritic dermatitis. TRPV3 dysfunction caused by genetic
74 gain-of-function mutations or pharmaceutical activation has been linked to human
75 skin diseases including genodermatosis known as Olmsted syndrome (Agarwala,
76 George, Pramanik, & McGrath, 2016; Lin et al., 2012) and erythromelalgia
77 (Duchatelet et al., 2014). Furthermore, TRPV3-deficient mice give rise to phenotypes
78 of curly whiskers and wavy hair coat (Cheng et al., 2010). Conversely, hyperactive
79 TRPV3 channels expressed in human outer root sheath keratinocytes inhibit hair
80 growth (Borbiro et al., 2011). While being implicated in a variety of skin disorders,
81 whether and how TRPV3 could be therapeutically targeted remains to be elucidated. It
82 is thus desirable to identify and understand clinical medications that can potentially
83 target TRPV3 channels.

84 As a clinical anesthetic, dyclonine is characterized by rapid onset of effect, lack of
85 systemic toxicity, and a low index of sensitization (Florestano & Bahler, 1956). Its
86 topical application (0.5% or 1% dyclonine hydrochloride contained in the topical
87 solution, i.e., ~30.7 mM at a dose of 1%, according to the United States Pharmacopeia)
88 rapidly relieves itching and pain in patients, by ameliorating inflamed, excoriated and
89 broken lesions on mucous membranes and skin (Morginson et al., 1956). Accordingly,
90 dyclonine is used to anesthetize mucous membranes prior to endoscopy (Formaker,
91 Mott, & Frank, 1998). The clinical scenario targeted by dyclonine treatment echoes

92 the pathological aspects of TRPV3-related skin disorders, suggesting that the
93 therapeutic effects of dyclonine might involve its interaction with TRPV3 sensory
94 channel.

95 Here, using a multidisciplinary approach combining electrophysiology, genetic
96 engineering and ultrafast local temperature control, we show that mouse and human
97 TRPV3 channel was potently suppressed by dyclonine. It dose-dependently inhibited
98 TRPV3 currents in a voltage-independent manner and rescued cell death caused by
99 TRPV3 gain-of-function mutation. In *vivo*, dyclonine indeed suppressed the
100 itching/scratching behaviors induced by TRPV3 channel agonist carvacrol as
101 evidenced by the TRPV3 knock out (KO) mice. At single-channel level, dyclonine
102 reduced TRPV3 channel open probability without altering the unitary conductance.
103 We also identified molecular residues that were capable of either eliminating or
104 enhancing the inhibitory effect of dyclonine. These data demonstrate the effective
105 inhibition of TRPV3 channel by dyclonine, supplementing a molecular mechanism
106 for its clinical effects and raising its potential to ameliorate TRPV3-associated
107 disorders.

108

109

110 **Results**

111 **Inhibition of TRPV3 currents by dyclonine**

112 We first examined the effect of dyclonine on TRPV3 activity induced by the TRPV
113 channel agonist 2-APB (100 μM). Whole-cell currents were recorded at a holding
114 potential of -60 mV in HEK 293T cells expressing mouse TRPV3. Because TRPV3
115 channels exhibit sensitizing properties upon repeated stimulation (Chung, Lee,
116 Mizuno, Suzuki, & Caterina, 2004a), we examined the effect of dyclonine after the
117 response had stabilized following repetitive application of 2-APB (Figure 1A). The
118 presence of 5 μM and 10 μM dyclonine significantly inhibited TRPV3 currents
119 response to $30 \pm 2\%$ and $15 \pm 3\%$ of control level, respectively. After washing out of
120 dyclonine, 2-APB evoked a similar response to the control level, indicating the
121 blocking effect of dyclonine is reversible (Figure 1A-B). We repeated the experiments
122 with different doses of dyclonine. The dose-response curve indicates that dyclonine
123 inhibited TRPV3 currents in a concentration-dependent manner with an IC_{50} of $3.2 \pm$
124 $0.24 \mu\text{M}$ ($n = 6$, Figure 1C). We further examined the inhibitory effect of dyclonine
125 on TRPV3 activated by varying concentrations of 2-APB (Figure 1D). The
126 dose-response curves to 2-APB were fitted with a Hill equation. The inhibitory effect
127 of dyclonine on TRPV3 activation was consistently observed under all tested 2-APB
128 concentrations (Figure 1E). The corresponding EC_{50} values and Hill coefficients were
129 not changed by the presence of dyclonine (Figure 1E, $\text{EC}_{50} = 22.93 \pm 0.02 \mu\text{M}$, $n_{\text{H}} =$
130 1.6 ± 0.1 without dyclonine vs. $\text{EC}_{50} = 22.03 \pm 0.86 \mu\text{M}$, $n_{\text{H}} = 1.7 \pm 0.1$ with 3 μM
131 dyclonine), as confirmed by the normalized dose-response curves (Figure 1F).

132 Therefore, dyclonine dose-dependently inhibits the response amplitudes of TRPV3
133 channel.

134 TRPV3 channel in physiological conditions has a low level of response to external
135 stimuli, which is augmented during the sensitization process (i.e., repetitive
136 stimulations, Figure 1A). In contrast, excessive up-regulation of TRPV3 activity
137 impairs hair growth and increases the incidence of dermatitis and pruritus in both
138 humans and rodents. To determine whether dyclonine affects the process of TRPV3
139 sensitization, TRPV3-expressing cells were repeatedly exposed to 100 μ M 2-APB
140 without or with 5 μ M dyclonine (Figure 1G-H). TRPV3 currents evoked by 2-APB
141 alone took \sim 8 repetitions to reach full sensitization level (Figure 1I). The presence of
142 dyclonine significantly slowed down this process, requiring \sim 16 repetitions to reach
143 the current level of full sensitization (Figure 1H-I). As expected, dyclonine also
144 reduced the initial TRPV3 current (31.12 ± 2.86 pA/pF, v.s. 86.43 ± 5.9 pA/pF
145 without dyclonine; $p < 0.001$; $n = 9$ per condition).

146 As TRPV3 is highly expressed in keratinocytes, we further determined the
147 inhibitory effect of dyclonine in primary mouse epidermal keratinocytes. After
148 stabilizing the channel current by repeated application of 2-APB, we tested the
149 inhibitory effect of 5 μ M and 30 μ M dyclonine (Figure 1J). On average, TRPV3
150 currents were reduced to $52 \pm 7\%$ and $13 \pm 0.01\%$ of control level by 5 μ M and 30
151 μ M dyclonine, respectively (Fig. 1K), reaching the similar level of inhibition by the
152 wide-spectrum TRP channel blocker ruthenium red (RR, Figure 1J). From the
153 dose-response curve (Figure 1L), the IC_{50} of dyclonine was assessed to be 5.2 ± 0.71

154 μM , with a Hill coefficient of $n_H = 2.4 \pm 0.75$ ($n = 7$). Thus, dyclonine effectively
155 suppresses the activity of endogenous TRPV3 channels in mouse keratinocytes.

156

157 **Dyclonine is a potent inhibitor of TRPV3 channel**

158 Next, we compared the inhibitory effect on TRPV3 of dyclonine to its impact on other
159 TRP channels. TRPV1, TRPV2, TRPM8 and TRPA1 channels were expressed in
160 HEK 293T cells and respectively activated by capsaicin, 2-APB, menthol and Allyl
161 Isothiocyanate (AITC). We observed that 10 μM dyclonine exhibited little inhibition
162 on TRPV1, TRPV2, TRPM8 and TRPA1, but potently inhibited TRPV3 channel
163 (Figure 2A). The corresponding reduction in current amplitude was $2 \pm 1\%$ for
164 TRPV1, $6 \pm 1\%$ for TRPV2, $9 \pm 2\%$ for TRPM8, $5 \pm 1\%$ for TRPA1, compared with
165 $87 \pm 1\%$ inhibition of TRPV3 current (Figure 2B). By applying a series of dyclonine
166 concentrations, we derived dose-response curves (Figure 2C). The corresponding IC_{50}
167 values of dyclonine for inhibiting TRPV1, TRPV2 TRPM8 and TRPA1 channels
168 ($336.3 \pm 12.0 \mu\text{M}$, $36.5 \pm 3.7 \mu\text{M}$, $72.4 \pm 10.9 \mu\text{M}$ and $152.35 \pm 16.3 \mu\text{M}$,
169 respectively) were one or two orders of magnitude higher than that for TRPV3
170 inhibition ($3.2 \pm 0.24 \mu\text{M}$), indicating that dyclonine represents an effective inhibitor
171 of TRPV3 channel.

172 Above results were obtained for mouse TRPV3. We further asked whether the
173 inhibitory effect of dyclonine on TRPV3 is consistent across different species.
174 Similarly, we performed whole-cell recordings in HEK 293T cells expressing human
175 TRPV3 and frog TRPV3, respectively. They were activated to a stable level by

176 repetitive 2-APB stimulation. Addition of dyclonine, indeed, efficiently suppressed
177 the activation of both types of TRPV3 channel (Figure 2D-I). Dose-response curves
178 for dyclonine inhibition yielded an IC_{50} value of $16.2 \pm 0.72 \mu\text{M}$ for hTRPV3 and
179 $12.3 \pm 1.6 \mu\text{M}$ for fTRPV3, respectively. Therefore, the inhibition of TRPV3 by
180 dyclonine is conserved across species.

181

182 **Inhibition of TRPV3 by dyclonine is voltage-independent**

183 To obtain a complete description of the inhibitory effect of dyclonine, we next
184 investigated its voltage dependence using a stepwise protocol (Figure 3A). We
185 measured membrane currents in TRPV3-expressing HEK 293T cells using a
186 Cs^+ -based pipette solution that blocks most outward K^+ channel current but permits
187 measurement of outward conductance mediated by the nonselective TRPV3 channel.
188 A low-concentration 2-APB ($40 \mu\text{M}$) activated small voltage-dependent currents with
189 steady-state outward rectification, characteristic of TRPV3 currents in heterologous
190 expression systems (Figure 3A). Addition of dyclonine in the extracellular solution
191 significantly diminished TRPV3-mediated outward and inward currents (Figure 3A).
192 By contrast, $10 \mu\text{M}$ ruthenium red, a broad TRP channel blocker, only inhibited
193 TRPV3-mediated inward currents but enhanced outward currents (Figure 3A), which
194 is consistent with early report (Cheng et al., 2010). Dyclonine inhibition of both
195 inward and outward currents was further confirmed by the I-V curves derived from
196 pooled data (Figure 3B). We found no significant difference inhibition at
197 hyperpolarized voltages versus depolarized voltages, showing the inhibition occurred

198 independently of the membrane potential (Figure 3C). Together, relative to the
199 wide-spectrum blocker ruthenium red, dyclonine more effectively inhibits TRPV3
200 channel in a voltage-independent manner.

201

202 **Inhibition of heat-activated TRPV3 currents by dyclonine**

203 TRPV3 is a thermal sensitive ion channel and has an activation threshold around 30 to
204 33 °C (Xu et al., 2002). We therefore explored whether the heat-evoked TRPV3
205 currents can be also inhibited by dyclonine. We employed an ultrafast infrared laser
206 system to control the local temperature near single cells; each temperature jump had a
207 rise time of 1.5 ms and lasted for 100 ms. TRPV3 sensitization of the channel was
208 induced by repeating a same temperature jump from room temperature to ~51 °C
209 (Figure 4A). TRPV3, expressed in HEK 293T cells, steadily responded to temperature
210 jumps ranging from 30 to 51 °C (Figure 4B). After pre-sensitization by repeated
211 temperature jumps from room temperature to 52 °C, application of dyclonine
212 appreciably inhibited TRPV3 thermal currents (Figure 4B-C). The inhibitory effect of
213 dyclonine was fully reversible, as after its washing out the TRPV3 response recovered
214 to the same level as control condition (Figure 4C). To determine the concentration
215 dependence of dyclonine inhibition, TRPV3 currents were evoked by a same
216 temperature jump from room temperature to ~52 °C in the presence of 1, 3, 5, 10, 30,
217 and 50 μM dyclonine (Figure 4D). The IC₅₀ of dyclonine on TRPV3 inhibition was
218 assessed to be 14.02 ± 2.5 μM with a Hill coefficient of $n_H = 1.9 \pm 0.54$, according to

219 the dose-response curve fitting (Figure 4E). These results thus indicate that dyclonine
220 dose-dependently suppresses heat-evoked TRPV3 currents.

221

222 **Dyclonine inhibited hyperactive TRPV3 mutants and rescued cell death**

223 It has previously been reported that gain-of-function mutations, G573S and G573C, of
224 TRPV3 are constitutively active and their expression causes cell death (Xiao, Tian,
225 Tang, & Zhu, 2008). We firstly examined the effect of dyclonine on the
226 electrophysiological activity of mutants. We transfected the inducible cDNA
227 constructs encoding respectively the GFP-tagged wild-type TRPV3, G573S, or G573
228 mutant into T-Rex 293 cells and then applied 20 ng/ml doxycycline to induce the gene
229 expression. As illustrated in Figure 5A and B, whole-cell recordings from G573S or
230 G573C expressed in T-Rex 293 cells show that spontaneous currents noticeably
231 appeared when changing the holding potential from 0 mV to -60 mV, and application
232 of 2-APB further increased the channel currents. In each patch, 20 μ M RR was
233 applied extracellularly to obtain remaining leak currents. By subtracting leak currents,
234 we found that spontaneous activities from G573S and G573C were reduced by $74 \pm 3\%$
235 ($n = 6$) and $71 \pm 2\%$ ($n = 6$) by 10 μ M dyclonine, respectively (Figure 5C). Also, the
236 presence of dyclonine significantly inhibited 300 μ M 2-APB-evoked responses to 10
237 $\pm 2\%$ (G573S, $n = 6$) and $11 \pm 1\%$ (G573C, $n = 6$) of control level (Figure 5D),
238 respectively. As both mutant TRPV3 channels are effectively inhibited by dyclonine,
239 we next explored whether it can rescue the cell death caused by these gain-of-function
240 mutants. Cells expressing G573S or G573S were exposed to different

241 pharmacological drugs (dyclonine, 2-APB, 2-APB and dyclonine, or ruthenium red).
242 Cell death was recognized by the narrow and contracted footprints in bright-field
243 images, and the protein expression meanwhile monitored by GFP fluorescence. As
244 shown in Figure 5E, massive cell death was seen in cells that expressed G573C and
245 G573S TRPV3 mutants but not those expressing the wild type TRPV3. Addition of
246 dyclonine largely prevented the cell death while not causing change in the expression
247 of TRPV3 channels (Figure 5E), indicating that dyclonine decreased the cytotoxicity
248 caused by the gain-of-function mutants. We further performed flow cytometry
249 analysis and observed that the cell death ratio was maintained at low level ($4.96 \pm$
250 0.87% , $n = 7$) in cells expressing wild-type TRPV3 (Figure 5F). By contrast, the
251 expression of G573S or G573C mutant significantly increased the cell death ratio to
252 $45.36 \pm 5.79\%$ ($n = 7$) and $52.74 \pm 4.94\%$ ($n = 7$), that were effectively reduced by
253 dyclonine ($50 \mu\text{M}$) to $12.45 \pm 2.54\%$ ($n = 7$) and $14.98 \pm 4.40\%$ ($n = 7$), respectively.
254 The cell-protective effect of dyclonine was mirrored by the general TRP channel
255 blocker ruthenium red (Figure 5E-G). As expected, activation of TRPV3 channels
256 with the agonist 2-APB caused significant cell death even in cells expressing
257 wild-type channel and exacerbated the cell death in those expressing the mutant
258 channel G573S or G573C (Figure 5G). Application of dyclonine also reversed the cell
259 death caused by 2-APB activation ($9.12 \pm 1.42\%$ vs. $43.73 \pm 3.46\%$ for wild-type
260 condition, $17.68\% \pm 5.66\%$ vs. $53.60 \pm 5.88\%$ for G573S, and $13.85\% \pm 2.49\%$ vs.
261 $47.91 \pm 5.54\%$ for G573C after and before addition of dyclonine). Collectively, these
262 results indicate that dyclonine rescues cell death by inhibiting the excessive activity of

263 TRPV3 channel.

264

265 **Dyclonine targets TRPV3 in vivo and ameliorates scratching behavior**

266 TRPV3 is highly expressed in skin keratinocytes, whose hyperactivity causes pruritic
267 dermatitis and scratching behavior. We next examined in vivo the therapeutic effect
268 of dyclonine on TRPV3 hyperactivity-caused scratching behavior in mouse model.
269 Itching-scratching behavior was induced by pharmacological activation of TRPV3
270 channel by a natural compound carvacrol derived from oregano (Cui, Wang, Wei, &
271 Wang, 2018). The number of scratching bouts was quantified every 5 min (Figure 6A),
272 and also summed over a 30-minute observation period (Figure 6B). Intradermal
273 injection of carvacrol (0.1%, 50 μ l) in wild-type TRPV3 mice caused significant
274 increases in the accumulated scratching bouts (137.2 ± 33.9) as compared to the
275 control group receiving normal saline (0.9% NaCl, 3.8 ± 1 , $n = 6$, $P < 0.001$; Figure
276 6B). By contrast, intradermal injection of carvacrol (0.1%, 50 μ l) did not elicit a
277 remarkable change in the number of scratching bouts in TRPV3^{-/-} mice (Figure 6A-B),
278 supporting that carvacrol caused itching-scratching behavior via TRPV3 activation
279 (Cui et al., 2018). To investigate whether dyclonine could alleviate carvacrol-evoked
280 acute itch, we made an intradermal injection of dyclonine into the mouse neck 30
281 minutes before the injection of carvacrol into the same site. As illustrated in Figure
282 6C-D, administration of 50 μ l dyclonine at 1, 10 and 50 μ M concentrations
283 appreciably reduced the scratching bouts to 130.0 ± 20.3 , 82.0 ± 15.0 , and 18.0 ± 8.0
284 from 137.8 ± 18.3 ($n = 6$), respectively. We also carried out whole-cell recordings in

285 TRPV3-expressing HEK 293T cells to further confirm the inhibitory effect of
286 dyclonine on TRPV3 currents activated by carvacrol. Similar to that observed with
287 the inhibition of 2-APB-evoked TRPV3 currents (Figure 1A-C), dyclonine also
288 inhibited carvacrol-activated TRPV3 currents in a concentration-dependent manner
289 with $IC_{50} = 3.5 \pm 0.34 \mu\text{M}$ following sensitization by repeated application of $300 \mu\text{M}$
290 2-APB ($n = 8$, Figure 6E-F), implying that the itching caused by carvacrol is mainly
291 due to the activation of TRPV3. Hence, dyclonine ameliorates TRPV3
292 hyperactivity-caused scratching in a concentration-dependent manner. In contrast,
293 dyclonine ($10 \mu\text{M}$) showed little effect on electrophysiological responses in mouse
294 dorsal root ganglia (DRG) and trigeminal ganglia (TG) neurons (Figure 6—figure
295 supplement 1). This observation is in line with the absence of TRPV3 in mouse DRGs
296 (Peier et al., 2002), and suggest that the in vivo effect of dyclonine arises from the
297 targeting of keratinocyte TRPV3 channels.

298 We also used wild-type and TRPV3 KO mice to examine the effect of dyclonine on
299 thermal nociceptive responses to the noxious temperature $55 \text{ }^\circ\text{C}$. In wild-type mice,
300 dyclonine exhibited a tendency to reduce the nociceptive response (Figure 6—figure
301 supplement 1). TRPV3 KO reduced mice nociceptive response to heating as
302 compared to wild-type mice ($55 \text{ }^\circ\text{C}$; comparison between gray bars in Figure
303 6—figure supplement 1E). However, in TRPV3 KO mice, dyclonine showed no
304 further effect, showing that dyclonine mainly targets TRPV3 in vivo. These
305 observations also suggest that TRPV3 partially contributes to pain sensation in

306 thermal nociception, in consistency with the temperature-dependent responses of
307 TRPV3 channel (Figure 4).

308

309 **Effects of dyclonine on single TRPV3 channel activity**

310 We then examined the functional and molecular mechanisms underlying the inhibition
311 of TRPV3 by dyclonine. To distinguish whether such inhibition arises from the
312 changes in channel gating or conductance, we measured single-channel activity.
313 Single-channel recordings were performed in an inside-out patch that was derived
314 from HEK 293T cells expressing the mouse TRPV3 (Figure 7). Currents were evoked
315 by 10 μM 2-APB in the absence and presence of dyclonine (30 μM) after sensitization
316 induced by 300 μM 2-APB at a holding potential of either +60 mV or -60 mV (Figure
317 7A). To quantify the changes, we constructed all-point histograms and measured the
318 open probabilities and the unitary current amplitudes by Gaussian fitting. We
319 observed that the single-channel open probability was largely decreased by dyclonine
320 from 0.8 ± 0.02 to 0.08 ± 0.01 at -60 mV and from 0.82 ± 0.02 to 0.12 ± 0.01 at +60
321 mV ($n = 6$), respectively (Figure 7B). Statistical analysis, however, revealed that
322 dyclonine had no effect on single TRPV3 channel conductance (163.6 ± 6.4 pS v.s.
323 179.2 ± 5.5 pS for before and after dyclonine treatment; Figure 7C).

324

325 **The mechanism underlying the inhibition of TRPV3 by dyclonine**

326 In order to understand the molecular mechanism underlying the blockade of TRPV3
327 by dyclonine, we utilized *in silico* docking to predict their interactions. The inhibitory
328 effect of drugs on ion channels is usually achieved in three ways, competitively
329 binding with agonists, negative allosteric regulation or directly blocking the channel
330 pore. Dyclonine inhibited TRPV3 currents evoked by both 2-APB (Figure 1) and heat
331 (Figure 4), implying that dyclonine is not a competitive antagonist. In addition, the
332 voltage independence of dyclonine inhibition and the fact that dyclonine is a positive
333 charged alkaloid suggests that dyclonine is not simply an open channel blocker.
334 Previous studies have demonstrated that local anesthetics inhibit voltage-gated
335 sodium channels through a common drug-binding region within the channel pore
336 (Tikhonov & Zhorov, 2017). We therefore suspected that the inhibition effect of
337 dyclonine is also due to its allosteric interaction with specific residues within the
338 aqueous pore of TRPV3. The grid file of *in silico* docking was then constructed to
339 examine residues in the upper pore region and the central cavity of TRPV3 (Figure
340 8—figure supplement 1A); the best receptor–ligand complex was evaluated using the
341 extra precision (XP) scoring. Ligand clusters derived from XP docking suggested
342 three potential TRPV3/dyclonine binding modes (BMs): BM_A, BM_B and BM_C (Figure
343 8A-B). Moreover, residues within 10 Å of dyclonine poses were extensively refined
344 using Induce-Fit-Docking (IFD) based on mTRPV3 cryo-EM structure (Singh,
345 McGoldrick, & Sobolevsky, 2018) (Figure 8A - Figure 8—figure supplement 1B).
346 BM_B and BM_C modes predicted that dyclonine occupies the ion permeation pathway
347 behaving as an open channel blocker. This, however, contradicts with the fact that

348 dyclonine is a positive charged alkaloid (Figure 8B) and its inhibition effect is
349 voltage-independent (Figure 3). Hence, BM_B and BM_C binding modes appear unlikely.
350 Nevertheless, mutants in key residues in these two binding sites diversely affected the
351 inhibition of dyclonine (I637A, $IC_{50} = 6.1 \pm 0.43 \mu M$; F666A, $IC_{50} = 414.5 \pm 15.7 \mu M$;
352 I674A, $IC_{50} = 15.1 \pm 2.1 \mu M$, Figure 8—figure supplement 1E-H), suggesting the
353 pore region is crucial for dyclonine inhibition.

354 BM_A mode shows that dyclonine makes contacts with the cavity formed by the pore
355 loop and S6-helix of TRPV3 (Figure 8A-B). Structures assigned to *apo* and open
356 states revealed remarkable allosteric changes and cavity size reduction in these
357 regions (Figure 8—figure supplement 1G-H), supporting the rationality of the BM_A
358 mode.

359 To further delineate dyclonine-interacting residues, we systematically mutated the
360 residues in the cavity of TRPV3 channel predicted by BM_A binding mode. Among the
361 mutants, mutations L630W, N643A, I644W and L655A greatly reduced the inhibitory
362 effect of dyclonine, whereas the mutants L642A and I659A showed higher sensitivity
363 to dyclonine than wild-type channel (Figure 8C-D). The dose-response curves were
364 fitted with a Hill equation, and the corresponding IC_{50} values for each TRPV3 mutant
365 were as follows: $IC_{50} = 286.7 \pm 10.4 \mu M$ for L655A; $IC_{50} = 30.8 \pm 2.2 \mu M$ for L630W;
366 $IC_{50} = 37.7 \pm 5.1 \mu M$ for N643A; $IC_{50} = 26.1 \pm 2.8 \mu M$ for I644W; $IC_{50} = 0.25 \pm$
367 $0.02 \mu M$ for L642A and $IC_{50} = 0.56 \pm 0.06 \mu M$ for I659A, compared to $IC_{50} = 3.2 \pm$
368 $0.24 \mu M$ for WT TRPV3 (Figure 8D-E). Notably, all mutant channels except L639A
369 were functional and produced robust responses to 2-APB (Figure 8F). Covalent

370 modification of L630C, F633C and L642C, with side chains toward the proposed
371 binding site, using MTSET (2-(trimethylammonium) ethyl methanethiosulfonate,
372 bromide), an MTS reagent with bulk positive side chain, significantly decreased
373 2-APB-induced current in the mutated mTRPV3 channels (Figure 8G-H). The
374 reduction reagent dithiothreitol (DTT) rescued this inhibitory effect, indicating that
375 the interruption of the allostery of the pore cavity has impaired the channel activation
376 of mTRPV3 (Figure 8G-H). In contrast, MTSET treatment had no effect on the
377 activation of wild-type TRPV3 (Figure 8H). Along the same line, MTSET
378 modification caused reduced dyclonine blockade in L630C, F633C and L642C but not
379 wild-type TRPV3, and DTT restored the blockage of dyclonine in these mutants
380 (Figure 8I), implying dyclonine-mediated inhibition is mediated by the region
381 predicted by BM_A binding mode. Together, our results suggest that dyclonine
382 interacts with the pore cavity of TRPV3 to prevent, likely behaving as a negative
383 allosteric modulator.

384

385 **Discussion**

386 As a multimodal sensory channel, TRPV3 is abundantly expressed in keratinocytes
387 and implicated in inflammatory skin disorders, itch, hair morphogenesis, and pain
388 sensation (Broad et al., 2016). Human Olmsted syndrome has been linked to the
389 gain-of-function mutations of TRPV3 (Agarwala et al., 2016; Lai-Cheong et al., 2012;
390 Lin et al., 2012). Synthetic and natural compounds, like isopentenyl pyrophosphate
391 (Bang, Yoo, Yang, Cho, & Hwang, 2011), 17(R)-resolvin D1 (Bang, Yoo, Yang, Cho,
392 & Hwang, 2012), forsythoside B (Zhang et al., 2019), diphenyltetrahydrofuran
393 osthole (Higashikawa et al., 2015) and ruthenium red (Xu et al., 2002) have been
394 proposed to inhibit TRPV3 channels. Due to either or both the lack of targeting
395 specificity and the clinical application, their remedial potential remains to be
396 determined. Hence, identifying and understanding clinical pharmaceuticals that target
397 TRPV3 channels will help to conceive therapeutic interventions.

398 Dyclonine is a topical antipruritic agent and has been used for clinical treatment of
399 itching and pain for decades (Gargiulo, Burns, & Huck, 1992; Greifenstein, Harris, &
400 Parry, 1956). While the therapeutic effect of dyclonine has been attributed to the
401 inhibition of cell depolarization, the underlying mechanisms have not been fully
402 understood. In the present study, we provide several tiers of evidence that dyclonine
403 potently inhibits TRPV3 channel. Such inhibition was observed for TRPV3 responses
404 to both chemical and thermal activation, suggesting dyclonine is a condition-across
405 inhibitor. Accordingly, dyclonine efficiently blocked the excessive activation of
406 TRPV3 mutants and prevented cell death. Single-channel recordings revealed that

407 dyclonine effectively suppresses the channel open probability without changing
408 single-channel conductance. These data not only supplement a molecular mechanism
409 for the therapeutic effect of dyclonine, but also suggest its application to curb
410 TRPV3-related disorders. Using mouse model, we indeed observed that dyclonin
411 ameliorates the TRPV3 hyperactivity-caused itch/scratching behaviors, indicating its
412 therapeutic inhibition effect being maintained *in vivo*. As TRPV3 responds to
413 moderate temperatures (30 - 40 °C), dyclonine may thus be used to alleviate skin
414 inflammations persisted in physiological temperatures. Also, as a clinical drug
415 dyclonine has been widely used and thus has shown its safety to human body
416 (Gargiulo et al., 1992; Sahdeo et al., 2014). In addition, as a potent inhibitor,
417 dyclonine can also be a research tool to dissect the physio- and pathological
418 characteristics of TRPV3 channel. While dyclonine effectively inhibits TRPV3
419 channels, our current results do not exclude its targeting of other molecular pathways.
420 For instance, voltage-gated sodium channels have been shown to be inhibited by local
421 anesthetics including dyclonine (Sahdeo et al., 2014; Tikhonov & Zhorov, 2017).

422 The current data also provide clues on the molecular mechanism underlying the
423 inhibition of TRPV3 by dyclonine. The residues within the pore loop and S6-helix of
424 TRPV3, as suggested by BM_A binding mode, create a functional ‘hotspot’ contributing
425 to the inhibition of dyclonine. Chemical modification experiment further confirmed
426 the importance of this ‘hotspot’ to channel gating and dyclonine inhibition.
427 Interestingly, the size of pocket BM_A is distinct in the apo/resting and open states.
428 Likely, binding of dyclonine into this pocket could prevent the structural

429 rearrangements of pore loop during TRPV3 gating, implying that dyclonine behaves
430 as a negative allosteric modulator. Although similar pockets can also be observed on
431 other TRP channels, the amino acids that make up the pocket and the precise shape of
432 the pocket are diverse (Figure 8—figure supplement 2). This may be the reason why
433 TRPV3 is targeted by dyclonine (Liao, Cao, Julius, & Cheng, 2013; Shimada et al.,
434 2020; Singh et al., 2018). F666 is located below the upper filter and behaves with a
435 bulky hydrophobic side chain, which may play a role in maintaining the shape of
436 BM_A at the open state. This may be the reason why F666A is capable of decreasing
437 the inhibition of dyclonine. Our current study revealed critical residues located within
438 the pore cavity of TRPV3 that regulate dyclonine inhibition, yet the possibility exists
439 that dyclonine inhibition is mediated by indirect mechanisms involving interactions
440 with other residues. Nevertheless, the molecular sites uncovered by the present study
441 would be instrumental for pinpointing the dyclonine-TRPV3 interaction at the
442 molecular level, thereby developing specific therapeutics for chronic pruritus,
443 dermatitis and skin inflammations.

Material and Methods

Key resources table

Reagent type (species) or resource	Designation	Source or reference	Identifiers	Additional information
Species (<i>Mus musculus</i>)	<i>Trpv3</i> ^{-/-} mice	(Wang et al., 2020)	PMID: 32535744	C57BL/6J background
Cell line (<i>Homo sapiens</i>)	HEK 293T	ATCC	Cat.#:CRL-32 16	
Cell line (<i>Homo sapiens</i>)	T-Rex 293	Thermo Fisher	Cat.#:R71007	
Chemical compound	2-APB	Sigma-Aldrich	Cat.#:D9754	TRPV1-3 agonist
Chemical compound	Carvacrol	MedChemExpress	Cat.#:499752	TRPV3 agonist
Chemical compound	Menthol	Sigma-Aldrich	Cat.#:M278	TRPM8 agonist
Chemical compound	Capsaicin	MedChemExpress	Cat.#: HY10448	TRPV1 agonist
Chemical compound	AITC	Sigma-Aldrich	Cat.#:377430	TRPA1 agonist
Chemical compound	Ruthenium Red	Sigma-Aldrich	Cat.#:R2751	TRP channels inhibitor
Chemical compound	Poly-L-lysi ne hydrochlori de	Sigma-Aldrich	Cat.#:2658	

Chemical compound	MTEST	MedChemExpress	Cat.#: 690632554
Chemical compound	DTT	Sigma-Aldrich	Cat.#: 3483123
Chemical compound	Dyclonine	MedChemExpress	Cat.#: 536436
Software, algorithm	Patchmaster	HEKA Electronics	
Software, algorithm	OriginPro	Originlab.com	
Software, algorithm	Clampfit 10	Molecular Devices	
Software, algorithm	SigmaPlot 10	SPSS Science	

445 **cDNA constructs and transfection in HEK 293T cells**

446 The wild-type mouse TRPV3 (mTRPV3), human TRPV3 (hTRPV3), rat TRPV1, rat
447 TRPV2, rat TRPM8 and mouse TRPA1 cDNAs were generously provided by Dr.
448 Feng Qin (State University of New York at Buffalo, Buffalo, USA). The
449 GFP-mTRPV3 wild-type and the mutants (mTRPV3-G573S and mTRPV3-G573C) in
450 pcDNA4/TO vector were gifts from Dr. Michael X. Zhu (The University of Texas
451 Health Science Center at Houston, Houston, USA). The wild-type frog TRPV3
452 (fTRPV3) was kindly provided by Dr. Makoto Tominaga (Department of
453 Physiological Sciences, SOKENDAI, Okazaki, Japan). All mutations were made
454 using the overlap-extension polymerase chain reaction (PCR) method as previously

455 described (Tian et al., 2019). The resulting mutations were then verified by DNA
456 sequencing. HEK 293T and T-Rex 293 cells were grown in Dulbecco's modified
457 Eagles medium (DMEM, Thermo Fisher scientific, MA, USA) containing 4.5 mg/ml
458 glucose, 10% heat-inactivated fetal bovine serum (FBS), 50 units/ml penicillin, and
459 50 mg/ml streptomycin, and were incubated at 37°C in a humidified incubator gassed
460 with 5% CO₂. For T-Rex 293, blasticidin S (10 µg/ml) was also included. Cells grown
461 into ~80% confluence were transfected with the desired DNA constructs using either
462 the standard calcium phosphate precipitation method or lipofectamine 2000
463 (Invitrogen) following the protocol provided by the manufacturer. Transfected HEK
464 293T cells were reseeded on 12 mm round glass coverslips coated by poly-L-lysine.
465 Experiments took place ~12-24 h after transfection.

466 **Cell lines**

467 HEK 293T and T-Rex 293 cell lines used in this study were respectively from the
468 American Type Culture Collection and Thermo Fisher, authenticated by STR locus
469 and tested negative for mycoplasma contamination.

470

471 **Mouse epidermal keratinocyte culture**

472 The animal protocol used in this study was approved by the Institutional Animal Care
473 and Use Committee of Wuhan University. Primary mouse keratinocytes were
474 prepared according to the method previously described (Luo, Stewart, Berdeaux, &
475 Hu, 2012; Pirrone, Hager, & Fleckman, 2005). Briefly, newborn wild-type C57B/6
476 mice (postnatal day 1–3) were deeply anaesthetized and decapitated and then soaked

477 in 10% povidone-iodine, 70% ethanol, and phosphate-buffered saline for 5 min,
478 respectively. The skin on the back was removed and rinsed with pre-cold sterile
479 phosphate-buffered saline (PBS) in a 100-mm Petri dish and transferred into a 2-ml
480 tube filled with pre-cold digestion buffer containing 4 mg/ml dispase II and incubated
481 overnight at 4 °C. After treatment with dispase II for 12-18 h, the epidermis was
482 gently peeled off from dermis and collected. Keratinocytes were dispersed by gentle
483 scraping and flushing with KC growth medium (Invitrogen, Carlsbad, CA). The
484 resulting suspension of single cells was collected by centrifuge and, cells were seeded
485 onto coverslips pre-coated with poly-L-lysine, and maintained in complete
486 keratinocyte serum-free growth medium (Invitrogen, Carlsbad, CA). Cell culture
487 medium was refreshed every two days. Patch-clamp recordings were carried out 48 h
488 after plating.

489 **Electrophysiological recording**

490 Conventional whole-cell and excised patch-clamp recording methods were used. For
491 the recombinant expressing system, green fluorescent EGFP was used as a surface
492 marker for gene expression. Recording pipettes were pulled from borosilicate glass
493 capillaries (World Precision Instruments), and fire-polished to a resistance between 2–
494 4 MΩ when filled with internal solution containing (in mM): 140 CsCl, 2.0 MgCl₂, 5
495 EGTA, 10 HEPES, pH 7.4 (adjusted with CsOH). Bath solution contained (in mM):
496 140 NaCl, 5 KCl, 3 EGTA, and 10 HEPES, pH 7.4 adjusted with NaOH. For
497 recordings in keratinocytes, the bath saline consisted of (in mM) 140 NaCl, 5 KCl, 2
498 MgCl₂, 2 CaCl₂, 10 glucoses, 10 HEPES, pH 7.4 adjusted with NaOH and the pipette

499 solution contained (in mM): 140 CsCl, 5 EGTA, and 10 HEPES, pH 7.3 adjusted with
500 CsOH. For single-channel recordings, the pipette solution and bath solution were
501 symmetrical and contained (in mM) 140 NaCl, 5 KCl, 3 EGTA, 10 HEPES, pH 7.4.
502 Isolated cells were voltage clamped and held at -60 mV using an EPC10 amplifier
503 with the Patchmaster software (HEKA, Lambrecht, Germany). For a subset of
504 recordings, currents were amplified using an Axopatch 200B amplifier (Molecular
505 Devices, Sunnyvale, CA) and recorded through a BNC-2090/MIO acquisition system
506 (National Instruments, Austin, TX) using QStudio developed by Dr. Feng Qin at State
507 University of New York at Buffalo. Whole-cell recordings were typically sampled at 5
508 kHz and filtered at 1 kHz, and single-channel recordings were sampled at 25 kHz and
509 filtered at 10 kHz. The compensation of pipette series resistance and capacitance were
510 compensated using the built-in circuitry of the amplifier (>80%) to reduce voltage
511 errors. Exchange of external solution was performed using a gravity-driven local
512 perfusion system. As determined by the conductance tests, the solution around a patch
513 under study was fully controlled by the application of a flow rate of 100 μ l/min or
514 greater. Dyclonine hydrochloride, MTSET (2-(trimethylammonium)ethyl
515 methanethiosulfonate, bromide) and carvacrol were purchased from MCE (Med Chem
516 Express). Unless otherwise noted, all chemicals were purchased from Sigma
517 (Millipore Sigma, St. Louis, MO). Water-insoluble reagents were dissolved in pure
518 ethanol or DMSO to make a stock solution and diluted into the recording solution at
519 the desired final concentrations before the experiment. The final concentrations of
520 ethanol or DMSO did not exceed 0.3%, which had no effect to currents. In the

521 scratching behavior experiments, carvacrol was firstly dissolved in 10% ethanol and
522 then diluted in normal saline before administration. All experiments except those for
523 heat activation were performed at room temperature (22-24°C).

524 **Ultrafast temperature jump achievement**

525 Rapid temperature jumps were generated by the laser irradiation approach as
526 described previously(Yao, Liu, & Qin, 2009). In brief, a single emitter infrared laser
527 diode (1470 nm) was used as a heat source. A multimode fiber with a core diameter of
528 100 μm was used to transmit the launched laser beam. The other end of the fiber
529 exposed the fiber core was placed close to cells as the perfusion pipette is typically
530 positioned. The laser diode driven by a pulsed quasi-CW current powder supply
531 (Stone Laser, Beijing, China). Pulsing of the controller was controlled from computer
532 through the data acquisition card using QStudio software developed by Dr. Feng Qin
533 at State University of New York at Buffalo. A blue laser line (460 nm) was coupled
534 into the fiber to aid alignment. The beam spot on the coverslip was identified by
535 illumination of GFP-expressing cells using the blue laser during experiment.

536 Constant temperature steps were generated by irradiating the tip of an open pipette
537 and using the current of the electrode as the readout for feedback control. The laser
538 was first powered on for a brief duration to reach the target temperature and was then
539 modulated to maintain a constant pipette current. The sequence of the modulation
540 pulses was stored and subsequently played back to apply temperature jumps to the
541 cell of interest. Temperature was calibrated offline from the pipette current using the

542 dependence of electrolyte conductivity.

543 **Cell death analysis by flow cytometry**

544 T-Rex 293 cells were grown in DMEM containing 4.5 mg/ml glucose, 10% (vol/vol)
545 FBS, 50 units/ml penicillin, 50 µg/ml streptomycin, and blasticidin S (10 µg/ml) and
546 were incubated at 37°C in a humidified incubator gassed with 5% CO₂. Transfections
547 were performed in wells of a 24-well plate using lipofectamine 2000 (Invitrogen). The
548 GFP-TRPV3 (wild-type and G573 mutants) cDNAs in pcDNA4/TO vector were
549 individually transfected into T-Rex 293 cells and treated with 20 ng/ml doxycycline
550 16 h post-transfection to induce the gene expression following the method as
551 previously described (Xiao et al., 2008). Expression of GFP fluorescence detected by
552 an epifluorescence microscope was used as an indicator of gene expression. After
553 treatments with the compounds for 12 h, cells were collected, washed twice with
554 phosphate-buffered saline (PBS), resuspended and then dyed with propidium iodide
555 (PI, Thermo Fisher Scientific) in the dark according to the manufacturer's instructions.
556 The membrane integrity of the cells was assessed using a BD FACSCelesta flow
557 cytometer equipped with BD Accuri C6 software (BD Biosciences, USA).

558 **Evaluation of scratching behavior in mice**

559 Behavioral studies were performed with six to eight-week-old wild-type or *Trpv3*^{-/-}
560 adult C57B/6 mice. To assess itch-scratching behaviors, the hair of the rostral part of
561 the mouse right neck was shaved using an electric hair clipper 24 hours before the
562 start of experiments. *Trpv3*^{-/-} mice have been described previously (Wang et al., 2020).

563 Scratching behaviors were recorded on video. The number of itch-scratching bouts
564 was counted through video playback analysis. One scratching bout was defined as an
565 episode in which a mouse lifted its right hind limb to the injection site and scratched
566 continuously for any time length until this limb was returned to the floor or mouth
567 (Wilson et al., 2013). All behavioral experiments were conducted in a double-blind
568 manner. To examine acute scratching/itch induced by carvacrol or pruritogen
569 histamine, mice were firstly placed in an observation box (length, width, and height: 9
570 $\times 9 \times 13$ cm³) for acclimatization for about 30 minutes. Then carvacrol (0.1%) in a
571 volume of 50 μ l was injected intradermally into the right side of the mouse neck. To
572 access the effect of dyclonine on itch scratching, normal saline (0.9% NaCl) or
573 dyclonine (1, 10, and 50 μ M) was injected intradermally 30 minutes before
574 intradermal injection of carvacrol (Cui et al., 2018; Sun & Dong, 2016). Behaviors
575 were recorded on video for 30 minutes following the injection of carvacrol.

576 **Hargreaves test for behavioral experiments**

577 All tests were conducted during the light phase of the light/dark cycle by a trained
578 observer blind to the genotype. Mice were habituated to the testing room for 60 min
579 prior to the behavioral tests unless otherwise stated. The Hargreaves test was
580 performed as described previously (Wang et al., 2018). All behavioral experiments
581 were conducted in a double-blind manner. For measure of thermal hyperalgesia,
582 animals were placed individually, 30 min after injection, on a hot plate (Bioseb,
583 Chaville, France) with the temperature adjusted to 55 °C. The withdrawal latency of

584 each hind paw was determined until nocifensive reaction appeared (licking foot).
585 Right hind paws of mice were injected intraplantarly with 10 μ l normal saline (0.9%
586 NaCl). Left hind paws of mice were injected intraplantarly with 10 μ l normal saline
587 (supplemented with 10 or 50 μ M dyclonine).

588 **Molecular docking**

589 The molecular docking approach was used to model the interaction between
590 dyclonine and TRPV3 channel protein (PDB ID code: 6DVZ) according to previous
591 description (L. D. Huang et al., 2014; Li et al., 2018). The 3D structure of dyclonine
592 was generated by LigPrep (Gadakar, Phukan, Dattatreya, & Balaji, 2007). Glide
593 (Friesner et al., 2004) and Induce-Fit-Docking (IFD) (Sherman, Day, Jacobson,
594 Friesner, & Farid, 2006) was employed to dock dyclonine into the potential binding.
595 For Glide docking, the grid for the protein was defined as an enclosing cubic box
596 within 34 Å to include upper pore region and the central cavity of TRPV3, and the
597 extra precision (XP) docking mode was selected. During in silico docking, at most
598 100000 poses passed through for the initial phase of docking, among of which top 300
599 poses were processed with post-docking minimization. The threshold for rejecting
600 minimized pose was set to 0.5 kcal/mol. A maximum of 200 poses were finally
601 written out. The docking scores and dyclonine-residue interaction distance were
602 summarized, sorted and then plotted by Maestro. Induced fit docking was performed
603 to refine the interaction between dyclonine and TRPV3 (Sherman et al., 2006), L655,
604 I674 and G638 residues were chosen from the center of the docking box, respectively.
605 During this docking process, the protein and the dyclonine were both flexible. All

606 structural figures were made by PyMol (<http://www.pymol.org>).

607 **Statistics**

608 Data were analyzed offline with Clampfit (Molecular Devices, Sunnyvale, CA),
609 IGOR (Wavemetrics, Lake Oswego, OR, USA), SigmaPlot (SPSS Science, Chicago,
610 IL, USA) and OriginPro (OriginLab Corporation, MA, USA). For concentration
611 dependence analysis, the modified Hill equation was used: $Y = A1 + (A2 - A1) / (1 +$
612 $(IC_{50} / [toxin])^{n_H})$, in which IC_{50} is the half maximal effective concentration, and n_H is
613 the Hill coefficient. Unless stated otherwise, the data are expressed as mean \pm
614 standard error (SEM), from a population of cells (n), with statistical significance
615 assessed by Student's t -test for two-group comparison or one-way analysis of variance
616 (ANOVA) tests for multiple group comparisons. Significant difference is indicated by
617 a p value less than 0.05 ($*p < 0.05$, $**p < 0.01$).

618 **Acknowledgements**

619 We are grateful to our colleagues and members of Yao lab for comments and
620 discussions, and we also would like to thank the core facilities of College of Life
621 Sciences at Wuhan University for technical help. This work was supported by grants
622 from the National Natural Science Foundation of China (31830031, 31929003,
623 31871174, 31671209 and 31601864), Natural Science Foundation of Hubei Province
624 (2017CFA063 and 2018CFA016), the Fundamental Research Funds for the Central
625 Universities, the Natural Science Foundation of Jiangsu Province (BK20202002),
626 Innovation and Entrepreneurship Talent Program of Jiangsu Province, and State Key
627 Laboratory of Utilization of Woody Oil Resource with grant number 2019XK2002.

628

629

630 **Conflict of Interest**

631 The authors declare that they have no conflict of interest.

632

633

634 **References**

- 635 Agarwala, M. K., George, R., Pramanik, R., & McGrath, J. A. (2016). Olmsted
636 syndrome in an Indian male with a new de novo mutation in TRPV3. *Br J*
637 *Dermatol*, *174*(1), 209-211. doi:10.1111/bjd.13910
- 638 Aijima, R., Wang, B., Takao, T., Mihara, H., Kashio, M., Ohsaki, Y., . . . Kido, M. A.
639 (2015). The thermosensitive TRPV3 channel contributes to rapid wound
640 healing in oral epithelia. *Faseb j*, *29*(1), 182-192. doi:10.1096/fj.14-251314
- 641 Asakawa, M., Yoshioka, T., Matsutani, T., Hikita, I., Suzuki, M., Oshima, I., . . .
642 Sakata, T. (2006). Association of a mutation in TRPV3 with defective hair
643 growth in rodents. *J Invest Dermatol*, *126*(12), 2664-2672.
644 doi:10.1038/sj.jid.5700468
- 645 Bang, S., Yoo, S., Yang, T. J., Cho, H., & Hwang, S. W. (2011). Isopentenyl
646 pyrophosphate is a novel antinociceptive substance that inhibits TRPV3 and
647 TRPA1 ion channels. *Pain*, *152*(5), 1156-1164. doi:10.1016/j.pain.2011.01.044
- 648 Bang, S., Yoo, S., Yang, T. J., Cho, H., & Hwang, S. W. (2012). 17(R)-resolvin D1
649 specifically inhibits transient receptor potential ion channel vanilloid 3 leading
650 to peripheral antinociception. *Br J Pharmacol*, *165*(3), 683-692.
651 doi:10.1111/j.1476-5381.2011.01568.x
- 652 Borbiri, I., Lisztes, E., Toth, B. I., Czifra, G., Olah, A., Szollosi, A. G., . . . Biro, T.
653 (2011). Activation of transient receptor potential vanilloid-3 inhibits human
654 hair growth. *J Invest Dermatol*, *131*(8), 1605-1614. doi:10.1038/jid.2011.122
- 655 Broad, L. M., Mogg, A. J., Eberle, E., Tolley, M., Li, D. L., & Knopp, K. L. (2016).

656 TRPV3 in Drug Development. *Pharmaceuticals (Basel)*, 9(3).
657 doi:10.3390/ph9030055

658 Cheng, X., Jin, J., Hu, L., Shen, D., Dong, X. P., Samie, M. A., . . . Xu, H. (2010).
659 TRP channel regulates EGFR signaling in hair morphogenesis and skin barrier
660 formation. *Cell*, 141(2), 331-343. doi:10.1016/j.cell.2010.03.013

661 Chung, M. K., Guler, A. D., & Caterina, M. J. (2005). Biphasic currents evoked by
662 chemical or thermal activation of the heat-gated ion channel, TRPV3. *J Biol*
663 *Chem*, 280(16), 15928-15941. doi:10.1074/jbc.M500596200

664 Chung, M. K., Lee, H., Mizuno, A., Suzuki, M., & Caterina, M. J. (2004a).
665 2-aminoethoxydiphenyl borate activates and sensitizes the heat-gated ion
666 channel TRPV3. *Journal of Neuroscience*, 24(22), 5177-5182.
667 doi:10.1523/Jneurosci.0934-04.2004

668 Chung, M. K., Lee, H., Mizuno, A., Suzuki, M., & Caterina, M. J. (2004b).
669 2-aminoethoxydiphenyl borate activates and sensitizes the heat-gated ion
670 channel TRPV3. *J Neurosci*, 24(22), 5177-5182.
671 doi:10.1523/JNEUROSCI.0934-04.2004

672 Chung, M. K., Lee, H., Mizuno, A., Suzuki, M., & Caterina, M. J. (2004c). TRPV3
673 and TRPV4 mediate warmth-evoked currents in primary mouse keratinocytes.
674 *J Biol Chem*, 279(20), 21569-21575. doi:10.1074/jbc.M401872200

675 Clapham, D. E. (2003). TRP channels as cellular sensors. *Nature*, 426(6966), 517-524.
676 doi:10.1038/nature02196

677 Colton, C. K., & Zhu, M. X. (2007). 2-Aminoethoxydiphenyl borate as a common

678 activator of TRPV1, TRPV2, and TRPV3 channels. *Handb Exp*
679 *Pharmacol*(179), 173-187. doi:10.1007/978-3-540-34891-7_10

680 Cui, T. T., Wang, G. X., Wei, N. N., & Wang, K. W. (2018). A pivotal role for the
681 activation of TRPV3 channel in itch sensations induced by the natural skin
682 sensitizer carvacrol. *Acta Pharmacologica Sinica*, 39(3), 331-335.
683 doi:10.1038/aps.2017.152

684 Duchatelet, S., Pruvost, S., de Veer, S., Fraitag, S., Nitschke, P., Bole-Feysot, C., . . .
685 Hovnanian, A. (2014). A new TRPV3 missense mutation in a patient with
686 Olmsted syndrome and erythromelalgia. *JAMA Dermatol*, 150(3), 303-306.
687 doi:10.1001/jamadermatol.2013.8709

688 Florestano, H. J., & Bahler, M. E. (1956). Antimicrobial properties of dyclonine
689 hydrochloride, a new topical anesthetic. *J Am Pharm Assoc Am Pharm Assoc*,
690 45(5), 320-325. doi:10.1002/jps.3030450514

691 Formaker, B. K., Mott, A. E., & Frank, M. E. (1998). The effects of topical anesthesia
692 on oral burning in burning mouth syndrome. *Ann N Y Acad Sci*, 855, 776-780.
693 doi:10.1111/j.1749-6632.1998.tb10657.x

694 Friesner, R. A., Banks, J. L., Murphy, R. B., Halgren, T. A., Klicic, J. J., Mainz, D.
695 T., . . . Shenkin, P. S. (2004). Glide: A new approach for rapid, accurate
696 docking and scoring. 1. Method and assessment of docking accuracy. *Journal*
697 *of Medicinal Chemistry*, 47(7), 1739-1749. Retrieved from <Go to
698 ISI>://WOS:000220317600019

699 Gadakar, P. K., Phukan, S., Dattatreya, P., & Balaji, V. N. (2007). Pose prediction

700 accuracy in docking studies and enrichment of actives in the active site of
701 GSK-3beta. *J Chem Inf Model*, 47(4), 1446-1459. doi:10.1021/ci6005036

702 Gao, L., Yang, P., Qin, P., Lu, Y., Li, X., Tian, Q., . . . Yao, J. (2016). Selective
703 potentiation of 2-APB-induced activation of TRPV1-3 channels by acid. *Sci*
704 *Rep*, 6, 20791. doi:10.1038/srep20791

705 Gargiulo, A. V., Burns, G. M., & Huck, C. P. (1992). Dyclonine hydrochloride--a
706 topical agent for managing pain. *Ill Dent J*, 61(4), 303-304. Retrieved from
707 <http://www.ncbi.nlm.nih.gov/pubmed/1286862>

708 Greifenstein, F. E., Harris, L. C., Jr., & Parry, J. C. (1956). Dyclonine; a new local
709 anesthetic agent: clinical evaluation. *Anesthesiology*, 17(5), 648-652.
710 doi:10.1097/00000542-195609000-00002

711 Higashikawa, A., Kojima, Y., Sato, M., Kimura, M., Ogura, K., Mochizuki, H., . . .
712 Tazaki, M. (2015). Transient Receptor Potential Cation Channel Subfamily
713 Vanilloid Member 3 is not Involved in Plasma Membrane Stretch-induced
714 Intracellular Calcium Signaling in Merkel Cells. *Bull Tokyo Dent Coll*, 56(4),
715 259-262. doi:10.2209/tdcpublish.56.259

716 Ho, J. C., & Lee, C. H. (2015). TRP channels in skin: from physiological implications
717 to clinical significances. *Biophysics (Nagoya-shi)*, 11, 17-24.
718 doi:10.2142/biophysics.11.17

719 Huang, L. D., Fan, Y. Z., Tian, Y., Yang, Y., Liu, Y., Wang, J., . . . Yu, Y. (2014).
720 Inherent dynamics of head domain correlates with ATP-recognition of P2X4
721 receptors: insights gained from molecular simulations. *PLoS One*, 9(5),

722 e97528. doi:10.1371/journal.pone.0097528

723 Huang, S. M., Lee, H., Chung, M. K., Park, U., Yu, Y. Y., Bradshaw, H. B., . . .
724 Caterina, M. J. (2008). Overexpressed transient receptor potential vanilloid 3
725 ion channels in skin keratinocytes modulate pain sensitivity via prostaglandin
726 E2. *J Neurosci*, 28(51), 13727-13737.
727 doi:10.1523/JNEUROSCI.5741-07.2008

728 Lai-Cheong, J. E., Sethuraman, G., Ramam, M., Stone, K., Simpson, M. A., &
729 McGrath, J. A. (2012). Recurrent heterozygous missense mutation,
730 p.Gly573Ser, in the TRPV3 gene in an Indian boy with sporadic Olmsted
731 syndrome. *Br J Dermatol*, 167(2), 440-442.
732 doi:10.1111/j.1365-2133.2012.11115.x

733 Li, B., Wang, J., Cheng, X. Y., Liu, Y., Yang, Y., Yang, X. N., . . . Yu, Y. (2018).
734 Molecular mechanism underlying the subtype-selectivity of competitive
735 inhibitor NF110 and its distinct potencies in human and rat P2X3 receptors.
736 *Science Bulletin*, 63(24), 1616-1625. Retrieved from <Go to
737 ISI>://WOS:000455135400008

738 Liao, M., Cao, E., Julius, D., & Cheng, Y. (2013). Structure of the TRPV1 ion channel
739 determined by electron cryo-microscopy. *Nature*, 504(7478), 107-112.
740 doi:10.1038/nature12822

741 Lin, Z., Chen, Q., Lee, M., Cao, X., Zhang, J., Ma, D., . . . Yang, Y. (2012). Exome
742 sequencing reveals mutations in TRPV3 as a cause of Olmsted syndrome. *Am*
743 *J Hum Genet*, 90(3), 558-564. doi:10.1016/j.ajhg.2012.02.006

744 Luo, J., & Hu, H. (2014). Thermally activated TRPV3 channels. *Curr Top Membr*, 74,
745 325-364. doi:10.1016/b978-0-12-800181-3.00012-9

746 Luo, J., Stewart, R., Berdeaux, R., & Hu, H. (2012). Tonic inhibition of TRPV3 by
747 Mg²⁺ in mouse epidermal keratinocytes. *J Invest Dermatol*, 132(9),
748 2158-2165. doi:10.1038/jid.2012.144

749 Moqrich, A., Hwang, S. W., Earley, T. J., Petrus, M. J., Murray, A. N., Spencer, K.
750 S., . . . Patapoutian, A. (2005). Impaired thermosensation in mice lacking
751 TRPV3, a heat and camphor sensor in the skin. *Science*, 307(5714),
752 1468-1472. doi:10.1126/science.1108609

753 Morginson, W. J., Rich, C. O., Eskelson, Y. D., Kirkman, L. W., Utterback, M.,
754 Burton, A. M., & Coletti, J. M. (1956). Dyclonine hydrochloride: a new
755 topical antipruritic agent. *Postgrad Med*, 19(6), 605-607.
756 doi:10.1080/00325481.1956.11708352

757 Peier, A. M., Reeve, A. J., Andersson, D. A., Moqrich, A., Earley, T. J., Hergarden, A.
758 C., . . . Patapoutian, A. (2002). A heat-sensitive TRP channel expressed in
759 keratinocytes. *Science*, 296(5575), 2046-2049. doi:10.1126/science.1073140

760 Pirrone, A., Hager, B., & Fleckman, P. (2005). Primary mouse keratinocyte culture.
761 *Methods Mol Biol*, 289, 3-14. doi:10.1385/1-59259-830-7:003

762 Sahdeo, S., Scott, B. D., McMackin, M. Z., Jasoliya, M., Brown, B., Wulff, H., . . .
763 Cortopassi, G. A. (2014). Dyclonine rescues frataxin deficiency in animal
764 models and buccal cells of patients with Friedreich's ataxia. *Hum Mol Genet*,
765 23(25), 6848-6862. doi:10.1093/hmg/ddu408

766 Sherman, W., Day, T., Jacobson, M. P., Friesner, R. A., & Farid, R. (2006). Novel
767 procedure for modeling ligand/receptor induced fit effects. *J Med Chem*, *49*(2),
768 534-553. doi:10.1021/jm050540c

769 Shimada, H., Kusakizako, T., Dung Nguyen, T. H., Nishizawa, T., Hino, T., Tominaga,
770 M., & Nureki, O. (2020). The structure of lipid nanodisc-reconstituted TRPV3
771 reveals the gating mechanism. *Nat Struct Mol Biol*, *27*(7), 645-652.
772 doi:10.1038/s41594-020-0439-z

773 Singh, A. K., McGoldrick, L. L., & Sobolevsky, A. I. (2018). Structure and gating
774 mechanism of the transient receptor potential channel TRPV3. *Nat Struct Mol*
775 *Biol*, *25*(9), 805-813. doi:10.1038/s41594-018-0108-7

776 Sun, S., & Dong, X. (2016). Trp channels and itch. *Semin Immunopathol*, *38*(3),
777 293-307. doi:10.1007/s00281-015-0530-4

778 Tian, Q., Hu, J., Xie, C., Mei, K., Pham, C., Mo, X., . . . Yao, J. (2019). Recovery
779 from tachyphylaxis of TRPV1 coincides with recycling to the surface
780 membrane. *Proc Natl Acad Sci U S A*, *116*(11), 5170-5175.
781 doi:10.1073/pnas.1819635116

782 Tikhonov, D. B., & Zhorov, B. S. (2017). Mechanism of sodium channel block by
783 local anesthetics, antiarrhythmics, and anticonvulsants. *J Gen Physiol*, *149*(4),
784 465-481. doi:10.1085/jgp.201611668

785 Wang, Y., Gao, Y., Tian, Q., Deng, Q., Wang, Y., Zhou, T., . . . Li, Y. (2018). TRPV1
786 SUMOylation regulates nociceptive signaling in models of inflammatory pain.
787 *Nat Commun*, *9*(1), 1529. doi:10.1038/s41467-018-03974-7

788 Wang, Y., Li, H., Xue, C., Chen, H., Xue, Y., Zhao, F., . . . Cao, Z. (2020). TRPV3
789 enhances skin keratinocyte proliferation through EGFR-dependent signaling
790 pathways. *Cell Biol Toxicol*. doi:10.1007/s10565-020-09536-2

791 Wilson, S. R., The, L., Batia, L. M., Beattie, K., Katibah, G. E., McClain, S. P., . . .
792 Bautista, D. M. (2013). The epithelial cell-derived atopic dermatitis cytokine
793 TSLP activates neurons to induce itch. *Cell*, *155*(2), 285-295.
794 doi:10.1016/j.cell.2013.08.057

795 Xiao, R., Tian, J., Tang, J., & Zhu, M. X. (2008). The TRPV3 mutation associated
796 with the hairless phenotype in rodents is constitutively active. *Cell Calcium*,
797 *43*(4), 334-343. doi:10.1016/j.ceca.2007.06.004

798 Xu, H., Delling, M., Jun, J. C., & Clapham, D. E. (2006). Oregano, thyme and
799 clove-derived flavors and skin sensitizers activate specific TRP channels. *Nat*
800 *Neurosci*, *9*(5), 628-635. doi:10.1038/nn1692

801 Xu, H., Ramsey, I. S., Kotecha, S. A., Moran, M. M., Chong, J. A., Lawson, D., . . .
802 Clapham, D. E. (2002). TRPV3 is a calcium-permeable temperature-sensitive
803 cation channel. *Nature*, *418*(6894), 181-186. doi:10.1038/nature00882

804 Yamada, T., Ueda, T., Ugawa, S., Ishida, Y., Imayasu, M., Koyama, S., & Shimada, S.
805 (2010). Functional expression of transient receptor potential vanilloid 3
806 (TRPV3) in corneal epithelial cells: involvement in thermosensation and
807 wound healing. *Exp Eye Res*, *90*(1), 121-129. doi:10.1016/j.exer.2009.09.020

808 Yamamoto-Kasai, E., Imura, K., Yasui, K., Shichijou, M., Oshima, I., Hirasawa, T., . . .
809 Yoshioka, T. (2012). TRPV3 as a therapeutic target for itch. *J Invest Dermatol*,

810 132(8), 2109-2112. doi:10.1038/jid.2012.97

811 Yao, J., Liu, B., & Qin, F. (2009). Rapid temperature jump by infrared diode laser

812 irradiation for patch-clamp studies. *Biophys J*, 96(9), 3611-3619.

813 doi:10.1016/j.bpj.2009.02.016

814 Zhang, H., Sun, X., Qi, H., Ma, Q., Zhou, Q., Wang, W., & Wang, K. (2019).

815 Pharmacological Inhibition of the Temperature-Sensitive and

816 Ca(2+)-Permeable Transient Receptor Potential Vanilloid TRPV3 Channel by

817 Natural Forsythoside B Attenuates Pruritus and Cytotoxicity of Keratinocytes.

818 *J Pharmacol Exp Ther*, 368(1), 21-31. doi:10.1124/jpet.118.254045

819

820

821 **Figure legends**

822 **Figure 1. Inhibition of TRPV3 currents by dyclonine.**

823 (A) Inhibition of 2-APB-evoked currents by dyclonine (Dyc) in a representative HEK
824 293T cell expressing mouse TRPV3. After sensitization by repeated application of
825 100 μM 2-APB, the cell was exposed to 5 or 10 μM dyclonine with 100 μM 2-APB
826 or 10 μM dyclonine only as indicated by the bars. Membrane currents were recorded
827 in whole-cell configuration, and the holding potential was -60 mV. (B) Summary of
828 relative currents elicited by 100 μM 2-APB in the presence of 0, 5 or 10 μM
829 dyclonine. Numbers of cells are indicated in parentheses. (C) The dose-response
830 curve for dyclonine inhibition of TRPV3 currents was fitted by Hill's equation ($\text{IC}_{50} =$
831 $3.2 \pm 0.24 \mu\text{M}$ and $n_{\text{H}} = 2.2 \pm 0.32$, $n = 6$). (D) Representative whole-cell current
832 traces showing the responses to varying concentrations of 2-APB without or with 3
833 μM dyclonine after full sensitization of TRPV3. (E) Concentration-response curves of
834 2-APB without or with dyclonine. Data are shown as relative values to the current
835 evoked by 300 μM 2-APB. Solid lines are fits to Hill equation, yielding $\text{EC}_{50} = 22.93$
836 $\pm 0.02 \mu\text{M}$ and $n_{\text{H}} = 1.6 \pm 0.1$ without dyclonine ($n = 6$); and $\text{EC}_{50} = 22.03 \pm 0.86 \mu\text{M}$
837 and $n_{\text{H}} = 1.7 \pm 0.1$ with 3 μM dyclonine ($n = 6$). (F) Dose-response curves normalized
838 to its own maximum of each condition. (G-H) Representative whole-cell recordings
839 for the sensitization of TRPV3 currents elicited by repeated applications of 100 μM
840 2-APB in the absence (G) and presence (H) of 5 μM dyclonine. (I) Time courses
841 toward the peak currents elicited by repeated application of 100 μM 2-APB with or
842 without dyclonine ($n = 9$). Currents were normalized to each initial values. (J) The

843 2-APB-evoked inward currents were reversibly inhibited by dyclonine in primary
844 mouse epidermal keratinocytes. Representative inward currents were firstly activated
845 by repeated application of 300 μM 2-APB at the holding potential of -60 mV, and then
846 inhibited by 5 or 30 μM dyclonine or 10 μM Ruthenium Red (RR) as indicated. **(K)**
847 Summary of relative currents elicited by 300 μM 2-APB with or without dyclonine.
848 **(L)** Dose dependence of dyclonine effects on TRPV3 currents in cultured
849 keratinocytes. The solid line corresponds to a fit by Hill's equation with $\text{IC}_{50} = 5.2 \pm$
850 $0.71 \mu\text{M}$ and $n_{\text{H}} = 2.4 \pm 0.75$ ($n = 6$). The dotted line indicates zero current level.

851

852 **Figure 2. Dyclonine is a potent inhibitor of TRPV3 channel.**

853 **(A)** Representative inward current traces from whole-cell voltage-clamp recordings
854 show the inhibitory effects of 10 μM dyclonine on TRPV1 (**A₁**), TRPV2 (**A₂**), TRPV3
855 (**A₃**), TRPM8 (**A₄**) or TRPA1 (**A₅**) channels (Dyc, dyclonine; Cap, capsaicin; Men,
856 menthol). Bars represent duration of drug application. **(B)** Summary of relative
857 currents before and after dyclonine (10 μM) treatment. Numbers of cells are indicated
858 in parentheses. **(C)** Dose-response curves of dyclonine for inhibition of indicated ion
859 channel currents. Solid lines represent fits by Hill equation, with $\text{IC}_{50} = 337.4 \pm 19.4$
860 μM and $n_{\text{H}} = 2.0 \pm 0.31$ for TRPV1 ($n = 7$), $\text{IC}_{50} = 31.1 \pm 2.7 \mu\text{M}$ and $n_{\text{H}} = 2.9 \pm 0.50$
861 for TRPV2 ($n = 8$), $\text{IC}_{50} = 81.8 \pm 12.7 \mu\text{M}$ and $n_{\text{H}} = 1.2 \pm 0.20$ for TRPM8 ($n = 6$),
862 $\text{IC}_{50} = 154.7 \pm 15.6 \mu\text{M}$ and $n_{\text{H}} = 1.3 \pm 0.15$ for TRPA1 ($n = 6$). For comparison, the
863 dose-response curve of TRPV3 channel from Figure 1C is displayed in red with IC_{50}
864 $= 3.2 \pm 0.24 \mu\text{M}$ and $n_{\text{H}} = 2.2 \pm 0.32$ ($n = 6$). **(D)** Suppression of 2-APB-evoked

865 currents by dyclonine in a hTRPV3-expressing HEK293T cell. Representative inward
866 current trace shows the reversible block effect of dyclonine (30 and 50 μM) at the
867 holding potential of -60 mV. (E) Summary of inhibition of hTRPV3 by dyclonine.
868 Membrane currents were normalized to the responses elicited by the saturated
869 concentration of 2-APB (100 μM) alone. (F) Dose-response curve for dyclonine on
870 blocking of hTRPV3. Solid line represents a fit to a Hill equation, yielded $\text{IC}_{50} = 16.2$
871 $\pm 0.72 \mu\text{M}$ and $n_{\text{H}} = 1.91 \pm 0.14$ ($n = 11$). (G) Inhibition of fTRPV3 currents by
872 dyclonine. Representative whole-cell currents at -60 mV in a fTRPV3-expressing
873 HEK293T cell. After sensitization by repeated application of 3 mM 2-APB, the cell
874 was exposed sequentially to 15 and 30 μM dyclonine with 3 mM 2-APB. (H)
875 Summary of inhibition of relative currents elicited by 3 mM 2-APB, 3 mM 2-APB
876 with dyclonine 15 or 30 μM . (I) Concentration-response curve of dyclonine on the
877 inhibition of fTRPV3 currents. Solid line represents a fit by a Hill equation, with IC_{50}
878 $= 12.31 \pm 1.6 \mu\text{M}$ and $n_{\text{H}} = 1.6 \pm 0.34$ ($n = 7$). The dotted line indicates zero current
879 level. Dyc, dyclonine; hTRPV3, human TRPV3; fTRPV3, frog TRPV 3.

880

881 **Figure 3. The inhibitory effect of dyclonine on TRPV3 channel is**
882 **voltage-independent.**

883 (A) Representative whole-cell currents evoked by voltage steps (*inset*) together with
884 40 μM 2-APB in the absence and presence of 10, 30 μM dyclonine or 10 μM RR in
885 HEK 293T cells expressing mouse TRPV3. Currents were elicited with 200-ms test

886 pulses ranging from -160 mV to +180 mV in 20-mV increments within the same cells,
887 and the holding potential was -60 mV. Calcium-free standard bath solution and a
888 CsCl-filled recording electrode were used. The dotted line indicates zero current level.
889 **(B)** Current-voltage relations for data in **(A)**. Current amplitudes were normalized to
890 the maximum responses at +180 mV in the presence of 40 μ M 2-APB. Each point
891 represents mean values (\pm SEM) from eight independent cells. (*Inset*) The inhibition
892 effects of dyclonine and RR on TRPV3 currents at negative holding potentials is
893 magnified and displayed on the right. Note that dyclonine had an inhibitory effect on
894 TRPV3 currents at both positive and negative potentials, but RR only inhibited
895 TRPV3 channel currents at negative potentials while enhanced TRPV3 currents at
896 positive potentials (blue trace). **(C)** Percentage block of TRPV3 currents by dyclonine
897 (10 and 30 μ M) as a function of membrane potential. Error bars represent SEM.

898

899 **Figure 4. Inhibition of heat-activated TRPV3 currents by dyclonine.**

900 **(A)** Sensitization of TRPV3 by heat. Heat-evoked TRPV3 currents in response to
901 repeated temperature jumps. Temperature pulse generated by infrared laser diode
902 irradiation was stepped from room temperature to 51 $^{\circ}$ C in 1.5 ms and then clamped for
903 100 ms. **(B)** Effects of dyclonine on heat-activated TRPV3 currents. Heat-evoked
904 current traces were recorded in whole-cell configuration, which were stabilized by
905 sensitization of repeated fast temperature jumps as shown in **(A)**. Temperature jumps
906 shown on the top had a duration of 100 ms and a rise time of 1.5 ms. Bath solution
907 with 0 or 30 μ M dyclonine was applied by brief perfusion to the patch just before

908 temperature stimulation on the same cells. (C) The average plot compares the
909 temperature responses in the absence and presence of 30 μM dyclonine (*Left*, $n = 6$).
910 Currents were normalized by their maximum responses under control condition,
911 respectively. Note that data from control and washout are superimposed. Percentage
912 block of heat-evoked TRPV3 currents by 30 μM dyclonine as a function of
913 temperature is shown on the right. (D) Representative inward currents evoked by a
914 series of identical temperature jumps inhibited by dyclonine in a
915 concentration-dependent manner. The temperature pulse (52 $^{\circ}\text{C}$) is shown in gray.
916 Holding potential was -60 mV. (E) Dose dependence of dyclonine effects on
917 heat-activated TRPV3 currents. The solid line represents a fit to Hill's equation with
918 $\text{IC}_{50} = 14.1 \pm 2.5 \mu\text{M}$ and $n_{\text{H}} = 1.9 \pm 0.54$ ($n = 10$). All whole-cell recordings were got
919 from TRPV3-expressing HEK 293T cells held at -60 mV.

920

921 **Figure 5. Dyclonine rescued cell death caused by expression of overactive TRPV3**
922 **mutant.**

923 (A-B) Effects of dyclonine on whole-cell currents recorded from TRPV3(G573S) and
924 TRPV3(G573C) expressed in T-Rex 293 cells, showing that dyclonine (3 and 10 μM)
925 reversibly inhibited the response to 300 μM 2-APB and the spontaneous activities at
926 -60 mV. 20 μM RR was applied for subtracting leak currents. Bars represent duration
927 of drug application. (C) Averaged inhibition of spontaneous activities of G573
928 mutants by dyclonine and RR. (D) Summary of relative whole-cell currents of

929 TRPV3(WT), G573S and G573S with or without dyclonine treatment. Error bars
930 represent SEM. (E) Bright field and fluorescence images showing the cell survival.
931 The GFP-tagged TRPV3 (wild-type, WT) and two mutants (G573C and G573S) in
932 pcDNA4/TO vector were respectively transfected into T-Rex 293 cells, and then
933 treated with doxycycline (20 ng/ml) for 16 h post-transfection to induce gene
934 expression in the presence of drugs as indicated. Images of cells were taken at 12 h
935 after induction. Scale bar, 50 μ m. (F) Flow cytometry analysis of the percentage of
936 dead cells. Cells transfected with the desired plasmids are as indicated. After the gene
937 expression induced by doxycycline, the cells were treated with dyclonine (Dyc, 50
938 μ M), 2-APB (30 μ M), ruthenium red (RR, 10 μ M) or the combination of 2-APB and
939 dyclonine, and then stained with propidium iodide, followed by flow cytometry to
940 analyze cell survival. (G) Summary plots of cell death rates under different treatments.
941 Data were averaged from seven independent experiments. *** $P < 0.0001$.

942

943 **Figure 6 Dyclonine suppresses scratching behavior induced by carvacrol.**

944 (A) Summary of the time courses of neck-scratching behaviors in wild-type TRPV3
945 and TRPV3 knock out (C57BL/6) mice after intradermal injection of 50 μ l carvacrol
946 (0.1%) or normal saline (0.9% NaCl) containing 0.1% ethanol into the mouse neck.
947 Time for scratching bouts was plotted for each five-minute interval over the 30
948 minutes observation period. (B) Quantification of the cumulative scratching bouts
949 over 30 minutes under different treatments, showing that intradermal injection of
950 carvacrol elicited a remarkable increase in the number of scratching bouts in

951 TRPV3^{+/+} but not TRPV3^{-/-} mice. ($n = 6$; N.S., no significance; $*P < 0.05$; $**P < 0.01$;
952 $***P < 0.001$, by one way ANOVA). (C) Time courses of neck-scratching behaviors
953 in response to intradermal injection of 50 μ l carvacrol (0.1%), with pretreatment of
954 normal saline (0.9% NaCl), or different concentrations (1, 10, 50 μ M) of dyclonine in
955 the same site. (D) Summary plots of the number of scratching bouts over 30 minutes
956 under different treatments as indicated, showing that dyclonine dose-dependently
957 alleviated carvacrol-evoked acute itch. ($n = 6$; N.S., no significance; $*P < 0.05$; $**P <$
958 0.01 ; $***P < 0.001$, by one way ANOVA). (E) Inhibition of carvacrol-evoked currents
959 by dyclonine (Dyc) in a representative HEK 293T cell expressing TRPV3. After
960 sensitization by repeated application of 300 μ M 2-APB, the cell was exposed to 3, 30
961 or 50 μ M dyclonine with 500 μ M Carvacrol as indicated by the bars. Membrane
962 currents were recorded in a whole-cell configuration, and the holding potential was
963 -60 mV. (F) The dose-response curve for dyclonine inhibition of carvacrol-evoked
964 TRPV3 currents was fitted by Hill's equation ($IC_{50} = 3.5 \pm 0.34 \mu$ M and $n_H = 2.1 \pm$
965 0.41 , $n = 8$).

966

967 **Figure 7. Effects of dyclonine on single channel properties of TRPV3.**

968 (A) Single-channel currents of TRPV3 were recorded from inside-out membrane
969 patches of HEK 293T cells at two membrane potentials (± 60 mV) in symmetrical 150
970 mM NaCl and were low-pass filtered at 2 kHz. Currents were evoked by 10 μ M
971 2-APB in the absence and presence of dyclonine (30 μ M) after sensitization induced
972 by repetitive 300 μ M 2-APB. All-point amplitude histograms of single-channel

973 currents were shown below the current traces. The histograms were fit to sums of two
974 Gaussian functions to determine the average amplitudes of currents and the open
975 probabilities. Dotted lines indicate the opened channel state (O) and the closed
976 channel state (C), respectively. **(B)** Summary of effects of dyclonine on TRPV3
977 single-channel open probability. Dyclonine (30 μ M) decreased TRPV3 open
978 probability from 0.8 ± 0.02 to 0.08 ± 0.01 at -60 mV ($n = 6$), and from 0.82 ± 0.02 to
979 0.12 ± 0.01 at +60 mV ($n = 6$), respectively. **(C)** I-V relationships of TRPV3
980 single-channel current evoked by 10 μ M 2-APB without (black triangles) and with 30
981 μ M dyclonine (red circles). Unitary conductance measured by fitting a linear function
982 were 163.6 ± 6.4 pS and 179.2 ± 5.5 pS for before and after treatment by dyclonine,
983 respectively.

984

985 **Figure 8. Molecular residues involved in dyclonine-TRPV3 interaction.**

986 **(A)** Overall view of the mTRPV3-dyclonine complex. Three putative binding modes
987 (BM) for dyclonine in the pore cavity of mTRPV3 channel (PDB ID code: 6DVZ) are
988 denoted as BM_A , BM_B and BM_C (please find the details in the text), with the
989 expanded view of BM_A shown on the right. Four subunits of the tetramer are
990 distinguished by different colors, and dyclonine in a schematic structure is shown in
991 red. **(B)** *Left*: potential docking poses of dyclonine and TRPV3 channel. *Right*: cluster
992 analysis showing all binding modes distributed into 3 clusters, BM_A , BM_B and BM_C .
993 **(C)** Representative whole-cell recordings show reversible blocking of 2-APB (1

994 mM)-evoked responses by dyclonine (3, 10 or 30 μ M) in HEK 293T cells expressing
995 mutant TRPV3 channels as indicated, respectively. The combination of 3, 10 or 30
996 μ M dyclonine and 2-APB was applied following the control currents evoked by a
997 saturated concentration of 2-APB (1 mM, initial grey bar). Holding potential was -60
998 mV. Bars represent duration of stimuli. **(D)** Concentration-response curves of
999 dyclonine on inhibition of the TRPV3 mutants. Solid lines represent fits by a Hill
1000 equation, with the half-maximal inhibitory concentration (IC_{50}) shown in **(E)**. For
1001 comparison, the dose-response curve of wild-type channel is displayed in gray. Four
1002 point mutations (L630W, N643A, I644W and L655A) reduced the inhibitory
1003 efficiency of dyclonine, while the other two point mutations (L642A and I659A)
1004 enhanced the inhibitory effects of dyclonine on TRPV3 currents. **(F)** Average current
1005 responses of mutant channels compared with wild-type TRPV3 channels. Each
1006 substitution of putative residues except L639A retained their normal responses to
1007 2-APB. Numbers of cells are indicated in parentheses. **(G)** Modulation of
1008 thiol-oxidizing and disulfide-reducing agents on the inhibitory effects of dyclonine.
1009 Whole-cell recordings from the wild-type TRPV3 and the mutants expressed in HEK
1010 293T cells, showing the effects of MTSET and DTT on the responses to 2-APB with
1011 or without dyclonine after sensitization induced by 300 μ M 2-APB. MTSET (1 mM)
1012 and DTT (10 mM) were locally applied for ~3 min to probe the accessibility,
1013 respectively. The responsiveness to 2-APB or 2-APB plus dyclonine was subsequently
1014 examined before and after treatments. Holding potential was -60 mV. **(H)** Summary of
1015 inhibition of relative currents elicited by 300 μ M 2-APB, 300 μ M 2-APB with

1016 dyclonine 10 or 1 μM . **(I)** Summary of inhibitory effects of dyclonine before and after
1017 treatments with MTSET and DTT. The dotted line indicates zero current level in all
1018 cases. Error bar represents SEM. N.S., no significance; * $P < 0.05$; ** $P < 0.01$; *** $P <$
1019 0.001.

1020

1021 **Figure 6—figure Supplement 1. Effects of dyclonine on the excitability of mouse**
1022 **DRG and TG neurons as well as the TRPV3-mediated nociceptive behavior.**

1023 **(A-B)** Current-clamp responses of DRG and TG neurons to 500 ms current pulse
1024 injection, respectively. Protocol of injected current is shown on the top. **(C)** Statistics
1025 plot showing no significant changes for RMP (resting membrane potential) from DRG
1026 or TG neurons in the presence of dyclonine (10 μM) compared with control. RMP
1027 were $-44 \pm 1.3 \text{ mV}$ ($n = 5$) vs. $-45 \pm 0.9 \text{ mV}$ ($n = 5$) treated with dyclonine in DRG
1028 neurons, and $-44.8 \pm 1.3 \text{ mV}$ ($n = 5$) vs. $-47.2 \pm 1.9 \text{ mV}$ ($n = 5$) treated with dyclonine
1029 in TG neurons. **(D)** Comparison of averaged frequency of action potential (AP) firing
1030 (numbers of action potential firing) evoked by current injection of 125 pA lasting for
1031 500 ms in DRG and TG neurons. **(E)** Paw withdrawal or licking latencies to noxious
1032 thermal stimuli at 55 $^{\circ}\text{C}$ evaluating the effect of dyclonine on thermal pain sensing.
1033 The paw withdrawal latencies (PWL) were $16.57 \pm 0.46 \text{ s}$ ($n = 12$), $18.08 \pm 0.03 \text{ s}$ (n
1034 $= 12$) and $18.82 \pm 0.42 \text{ s}$ ($n = 12$) for hind paws with intraplantar injection with saline,
1035 10 μM and 50 μM dyclonine in *TRPV3*^{+/+} mice, respectively. The PWL were $18.93 \pm$
1036 0.61 s ($n = 12$), $18.23 \pm 0.52 \text{ s}$ ($n = 12$), and $18.61 \pm 0.46 \text{ s}$ ($n = 12$) for hind paws

1037 with intraplantar injection with saline, 10 μ M and 50 μ M dyclonine in *TRPV3*^{-/-} mice.

1038 N.S., no significance; **P* < 0.05; ***P* < 0.01; ****P* < 0.001.

1039

1040 **Figure 8—figure supplement 1. Residues in the TRPV3 channel pore for**
1041 **interacting with dyclonine.**

1042 (A) Receptor grid for docking generated with 35 Å × 35 Å × 35 Å dimensions. (B)

1043 Detailed binding modes of dyclonine in BM_B and BM_C. The putative interaction

1044 residues are labeled and dyclonine is displayed in sticks for emphasis. (C)

1045 Representative whole-cell recordings show reversible blocking of 2-APB (1

1046 mM)-evoked responses by dyclonine (10 or 30 μ M) in HEK 293T cells expressing

1047 mutant TRPV3 channels as indicated, respectively. Holding potential was -60 mV.

1048 Bars represent duration of stimuli. (D) Concentration-response curves of dyclonine on

1049 inhibition of the TRPV3 mutants. Solid lines represent fits by a Hill equation, with the

1050 half-maximal inhibitory concentration (IC₅₀) shown in (E). For comparison, the

1051 dose-response curve of wild-type is displayed in gray. (F) Average current responses

1052 of mutant channels compared with wild-type TRPV3 channels. Only cells that

1053 expressed I637A, F666A or I674A showed similar response as wild-type channel,

1054 while others with the substitution by alanine were not functional. Numbers of cells are

1055 indicated in parentheses. (G) Structures assigned to apo/resting (left) and open states

1056 (right). (H) Cavity fostered by the pore helix and S5-S6 domains of TRPV3 channels

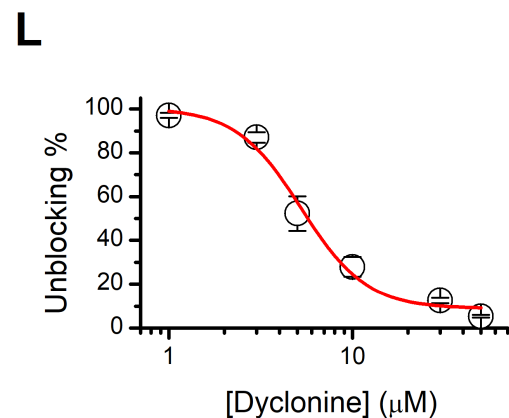
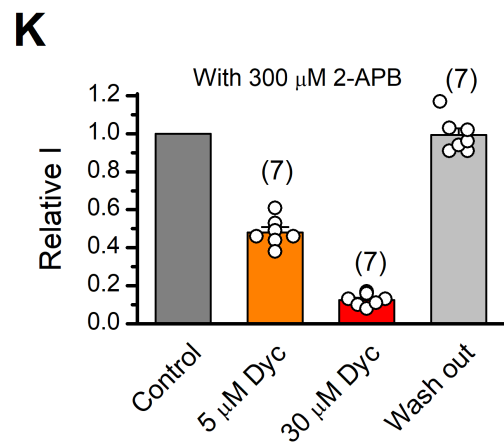
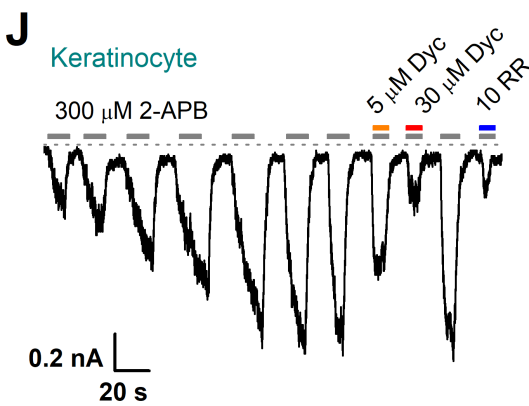
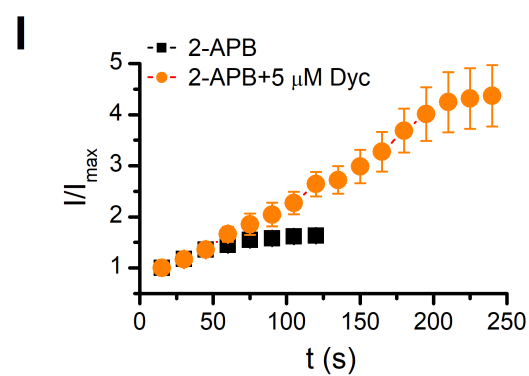
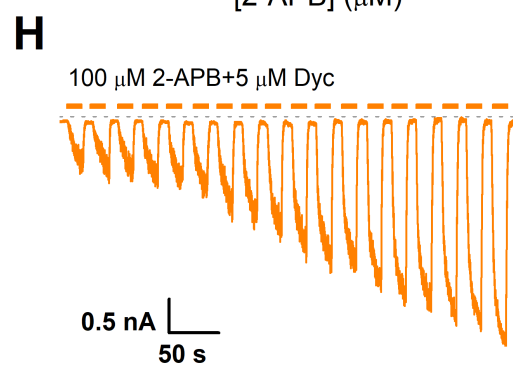
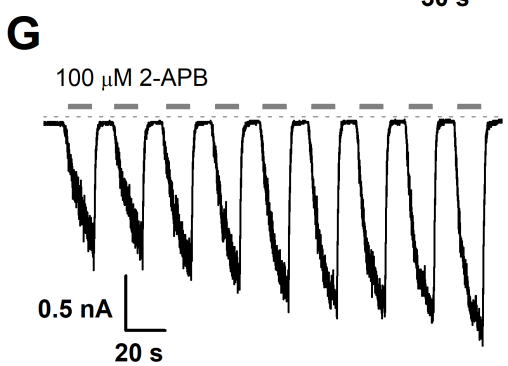
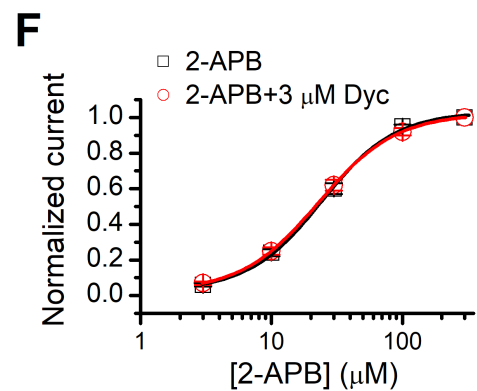
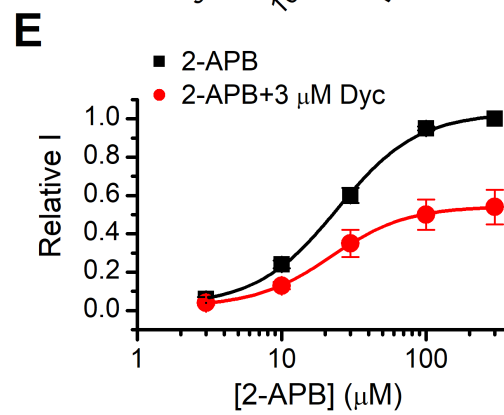
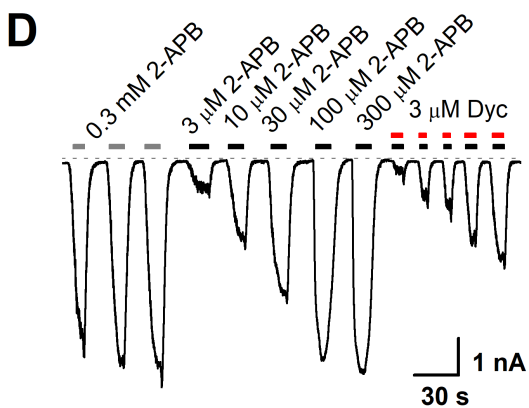
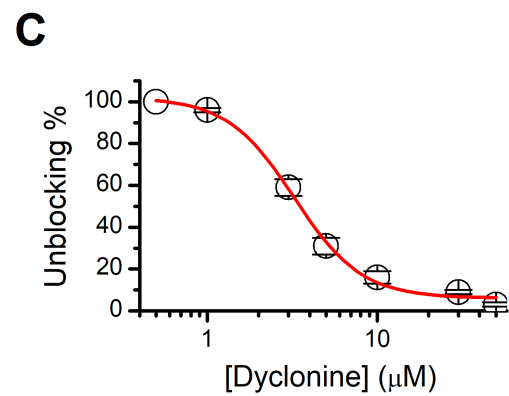
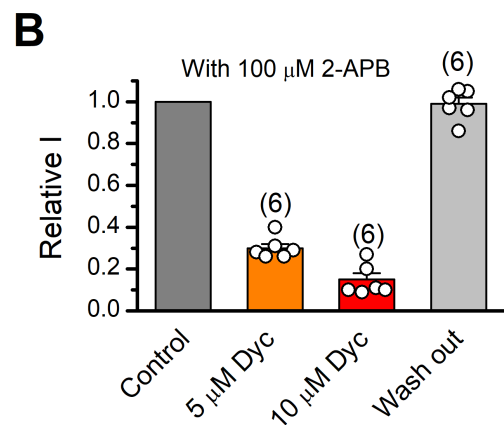
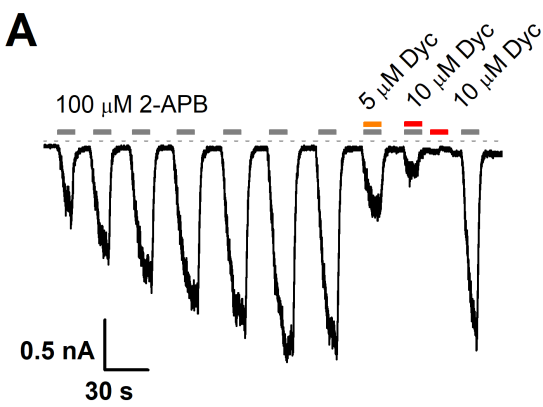
1057 at the resting (left) and open (right) states.

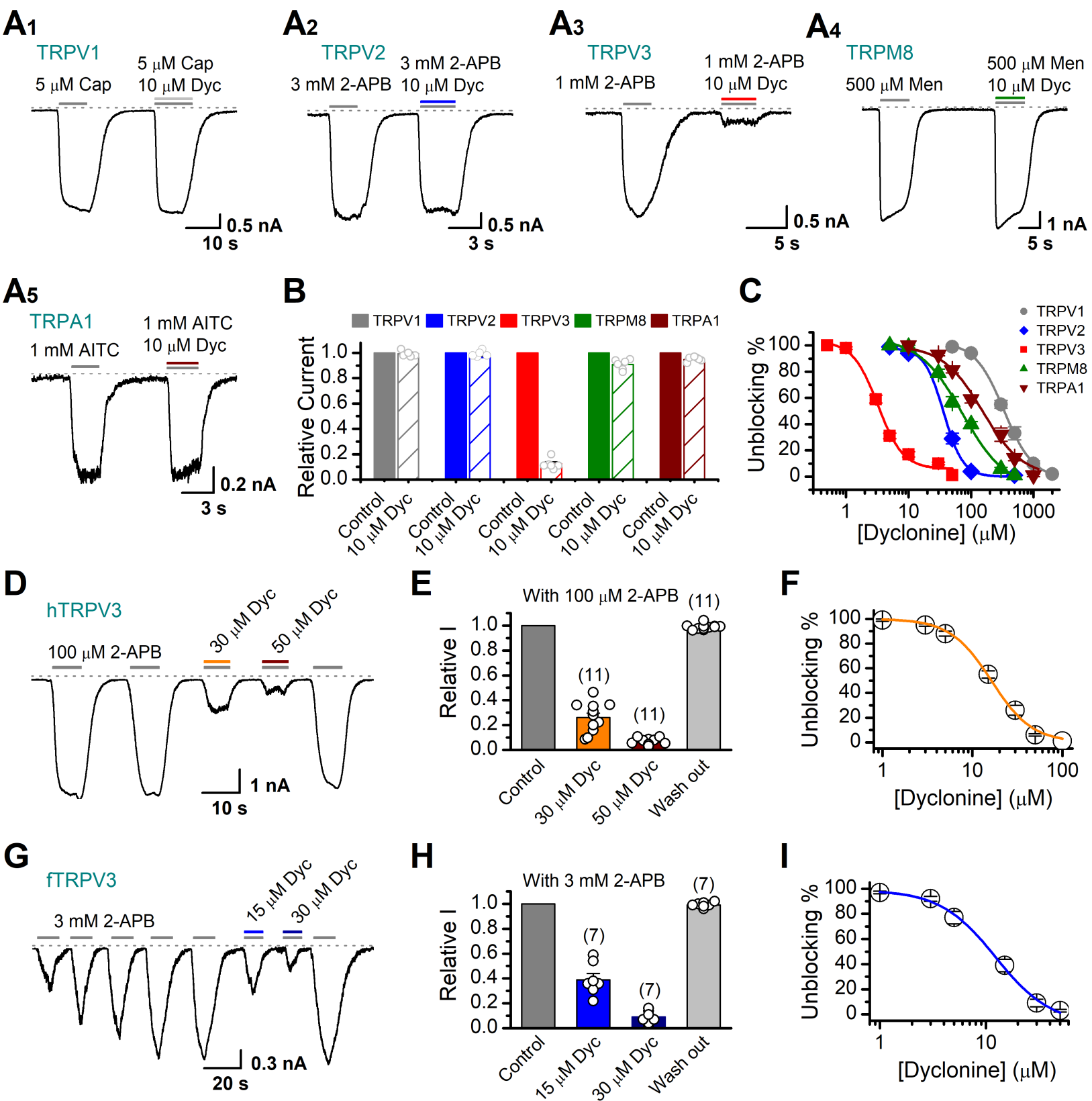
1058

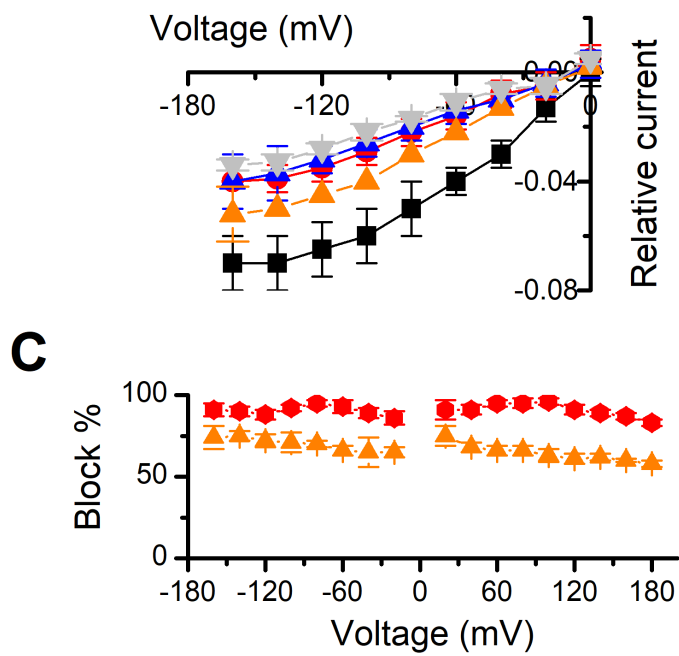
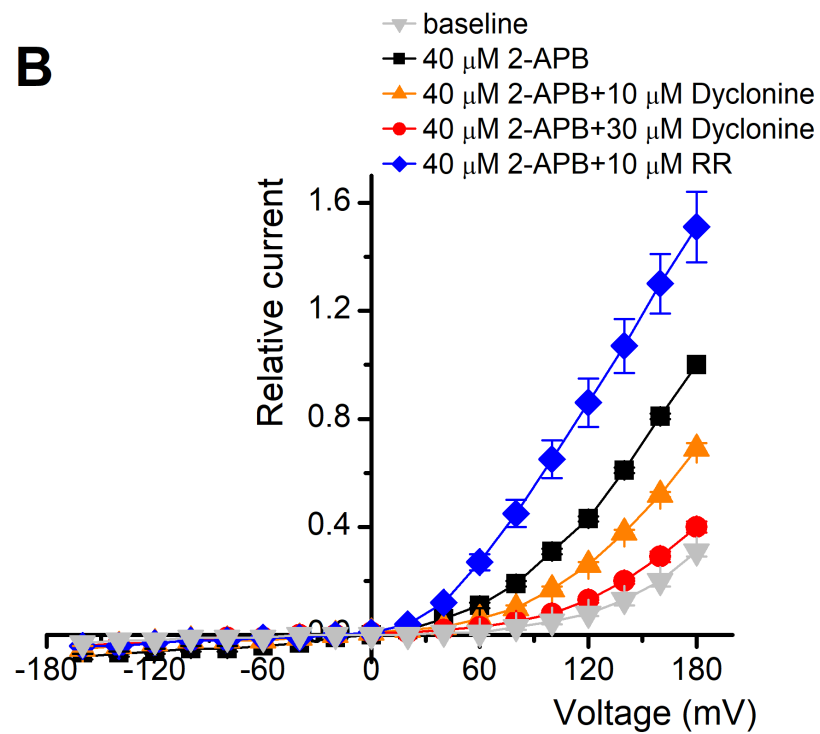
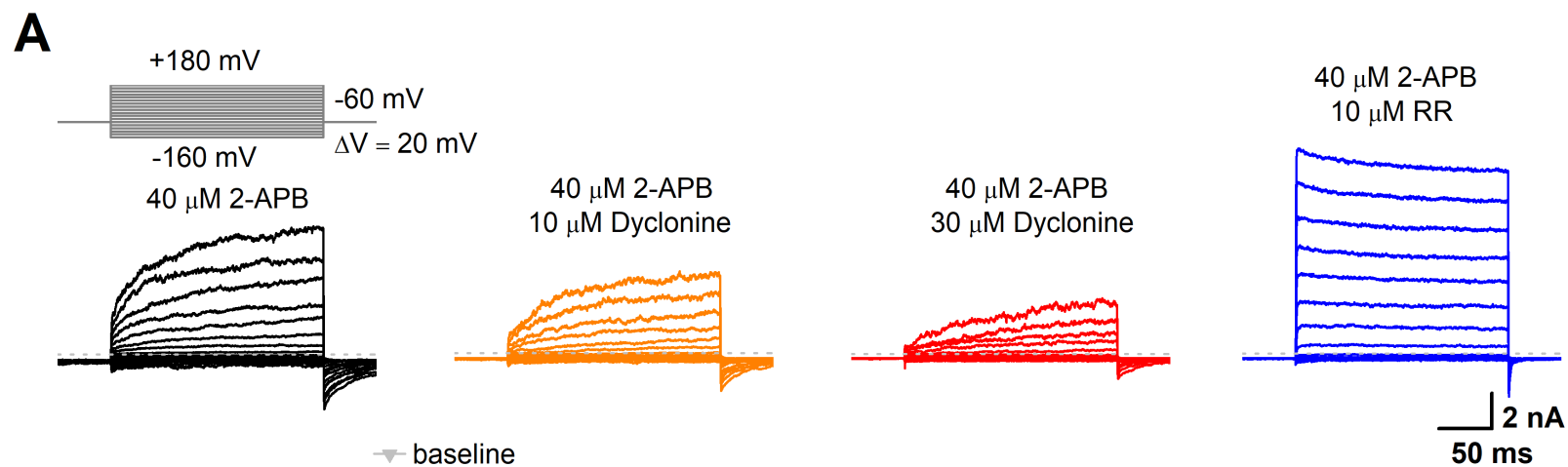
1059 **Figure 8—figure supplement 2. Alignment of the pore-region sequences.**

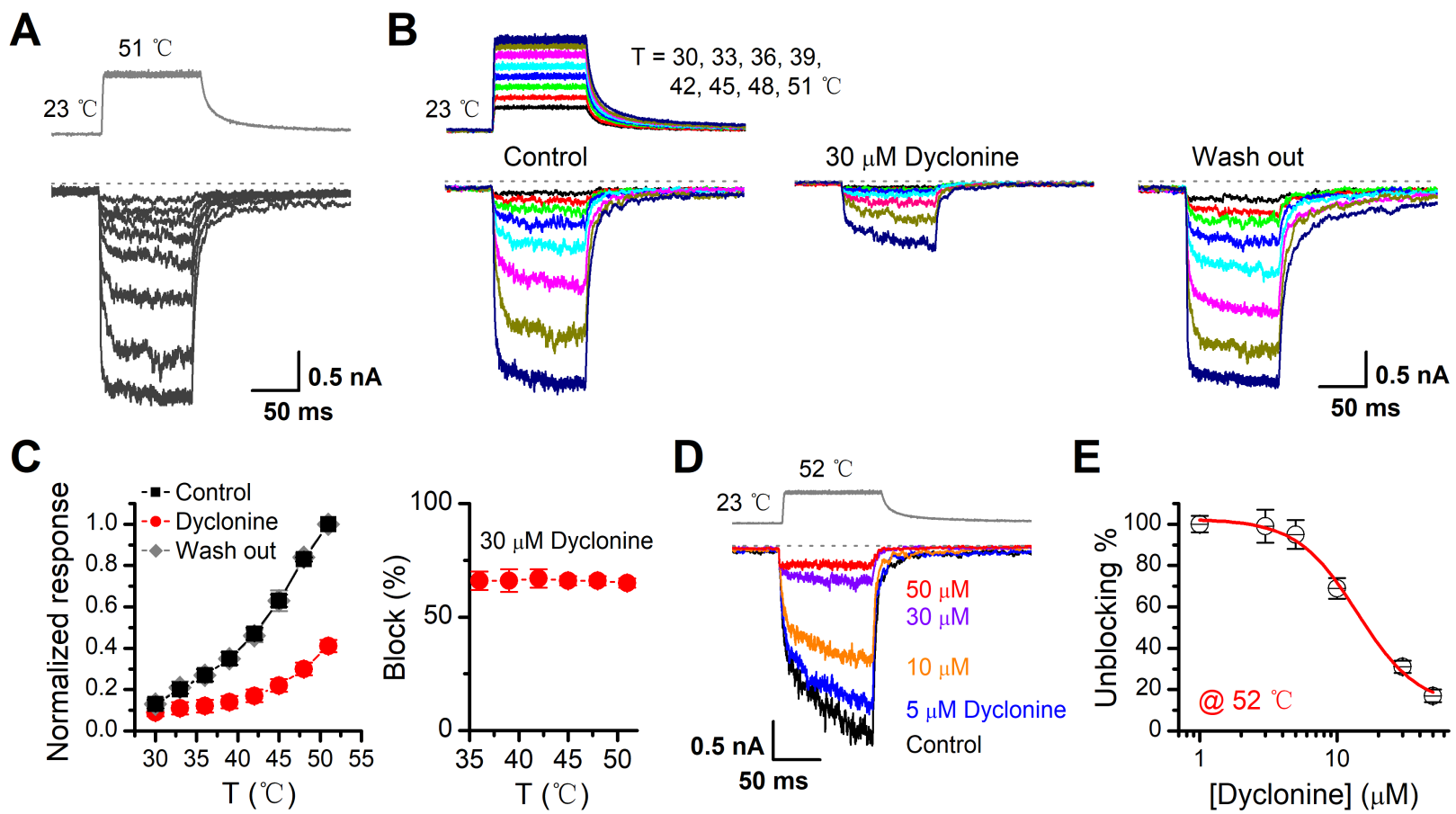
1060 Alignment of the pore sequence of mTRPV3 with other TRP channels, with the
1061 identical or similar residues shaded in colors. Meanwhile, differences in amino acids
1062 compositions present for different channels. The key residues of TPRV3 are indicated
1063 at the top, which affects the inhibitory effect of dyclonine.

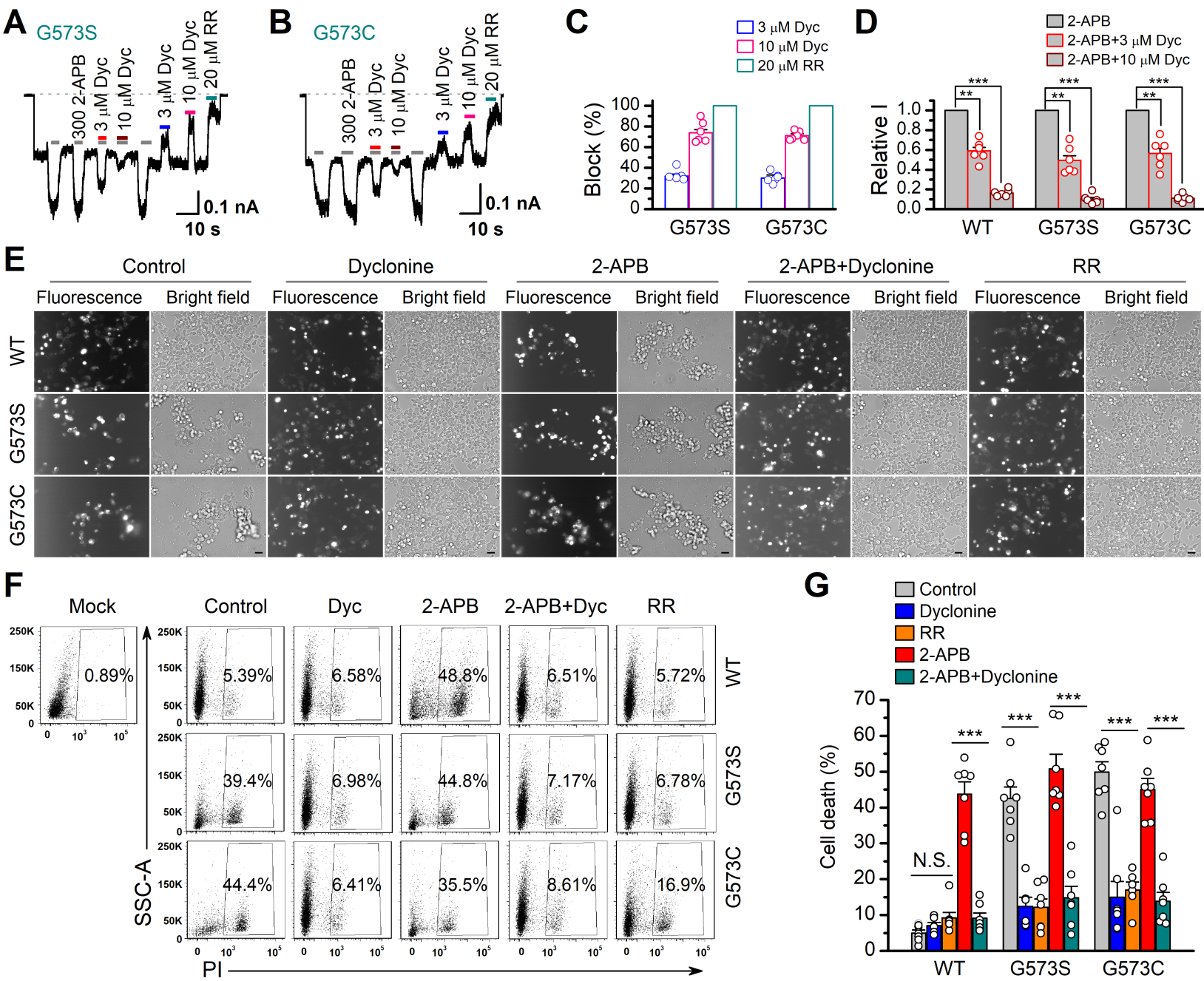
1064

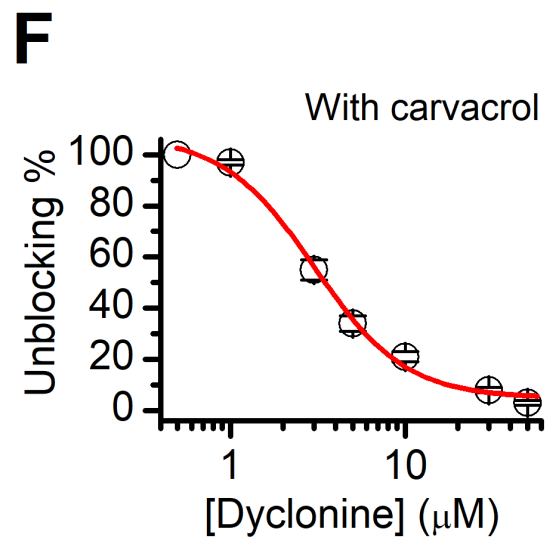
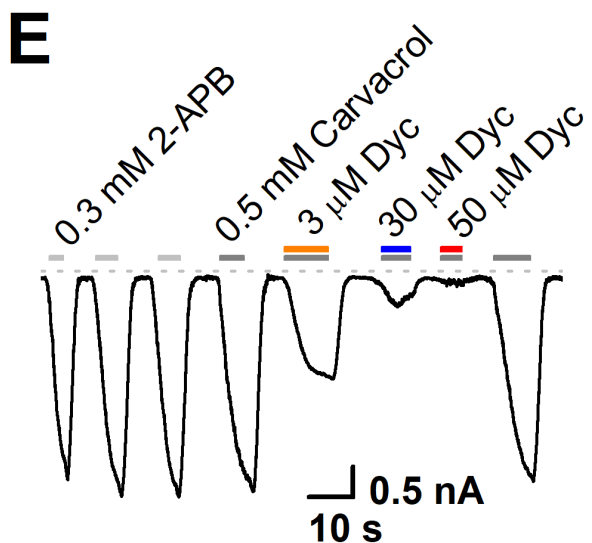
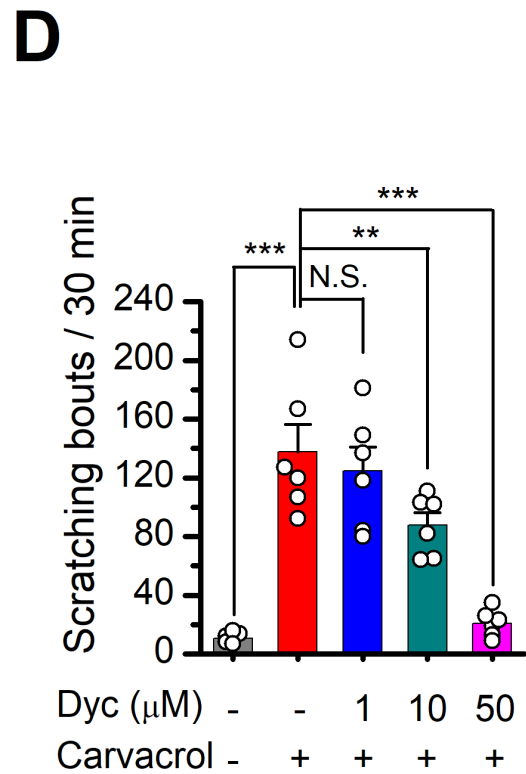
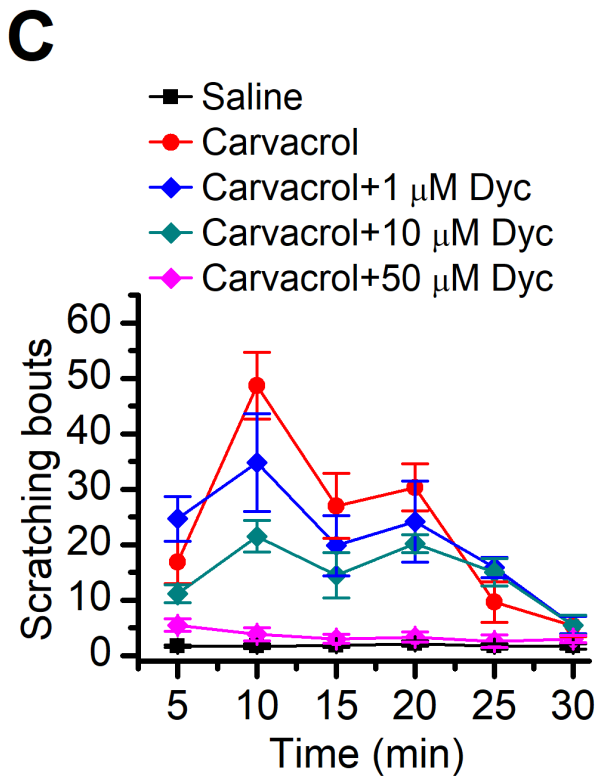
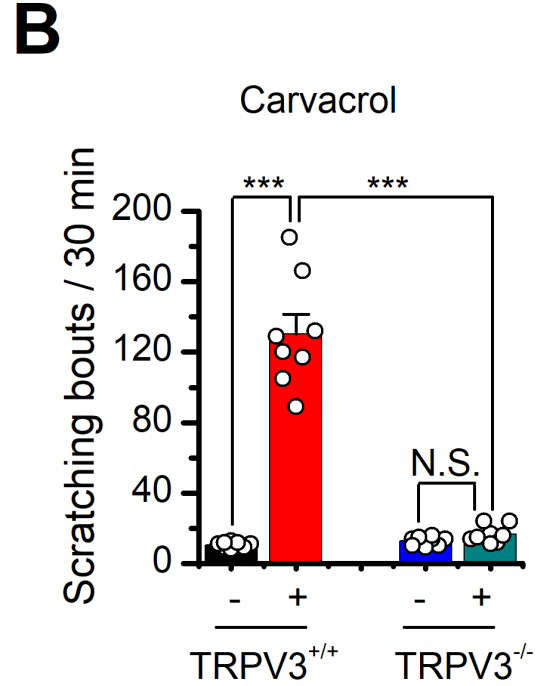
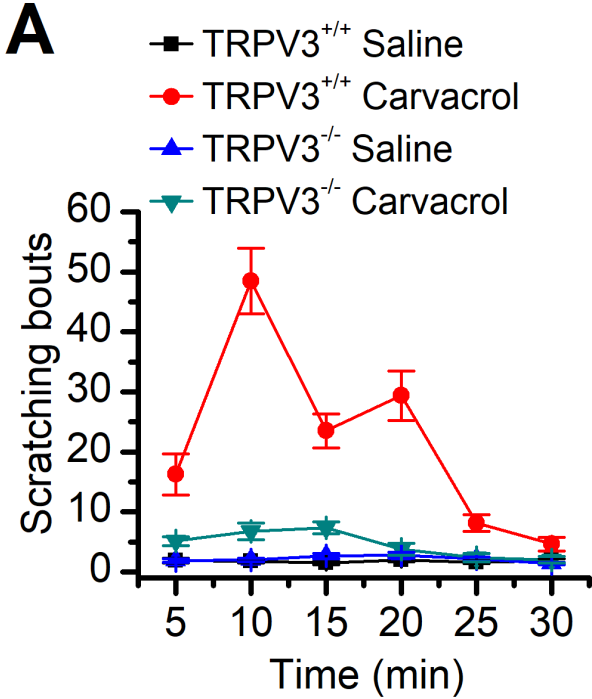


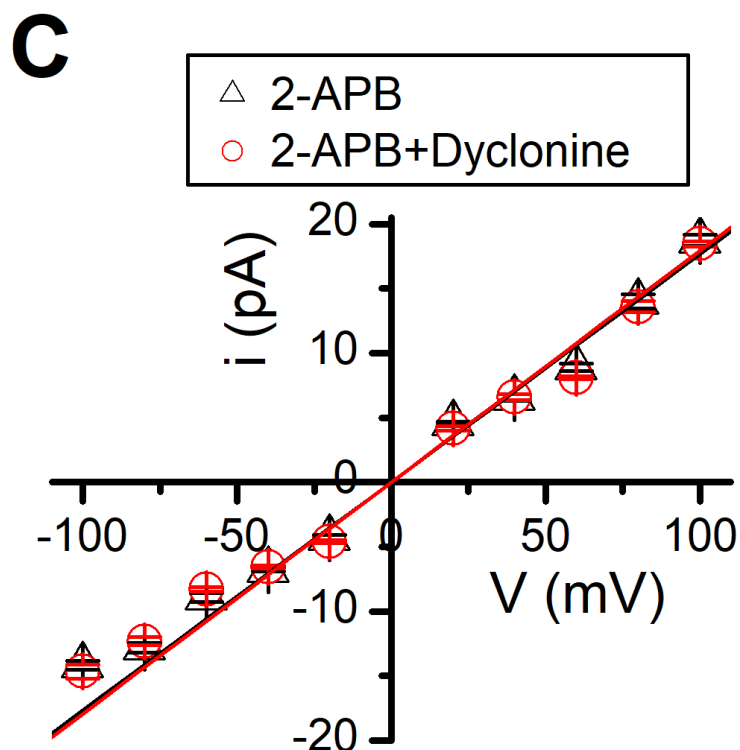
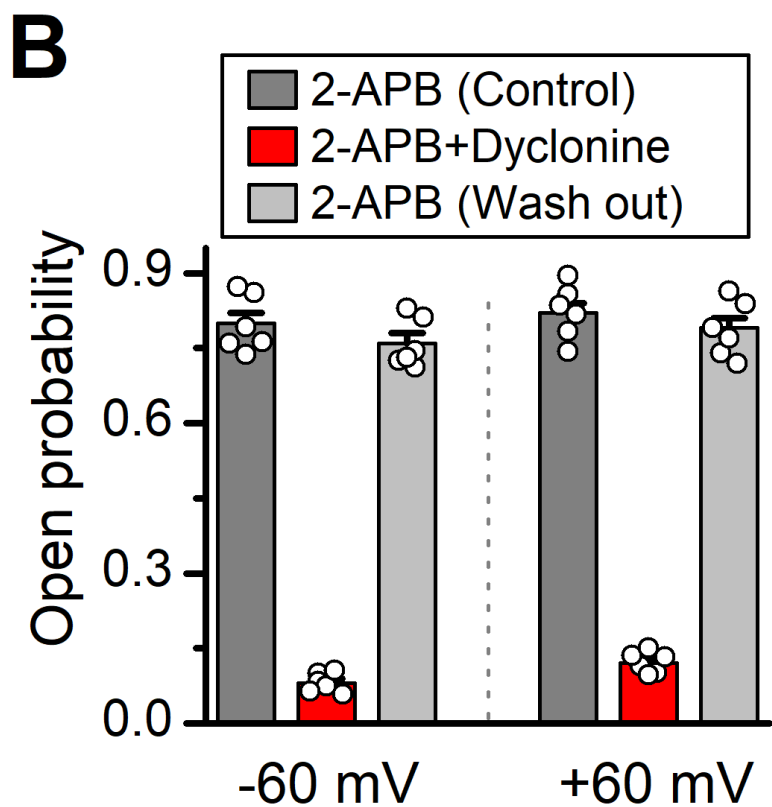
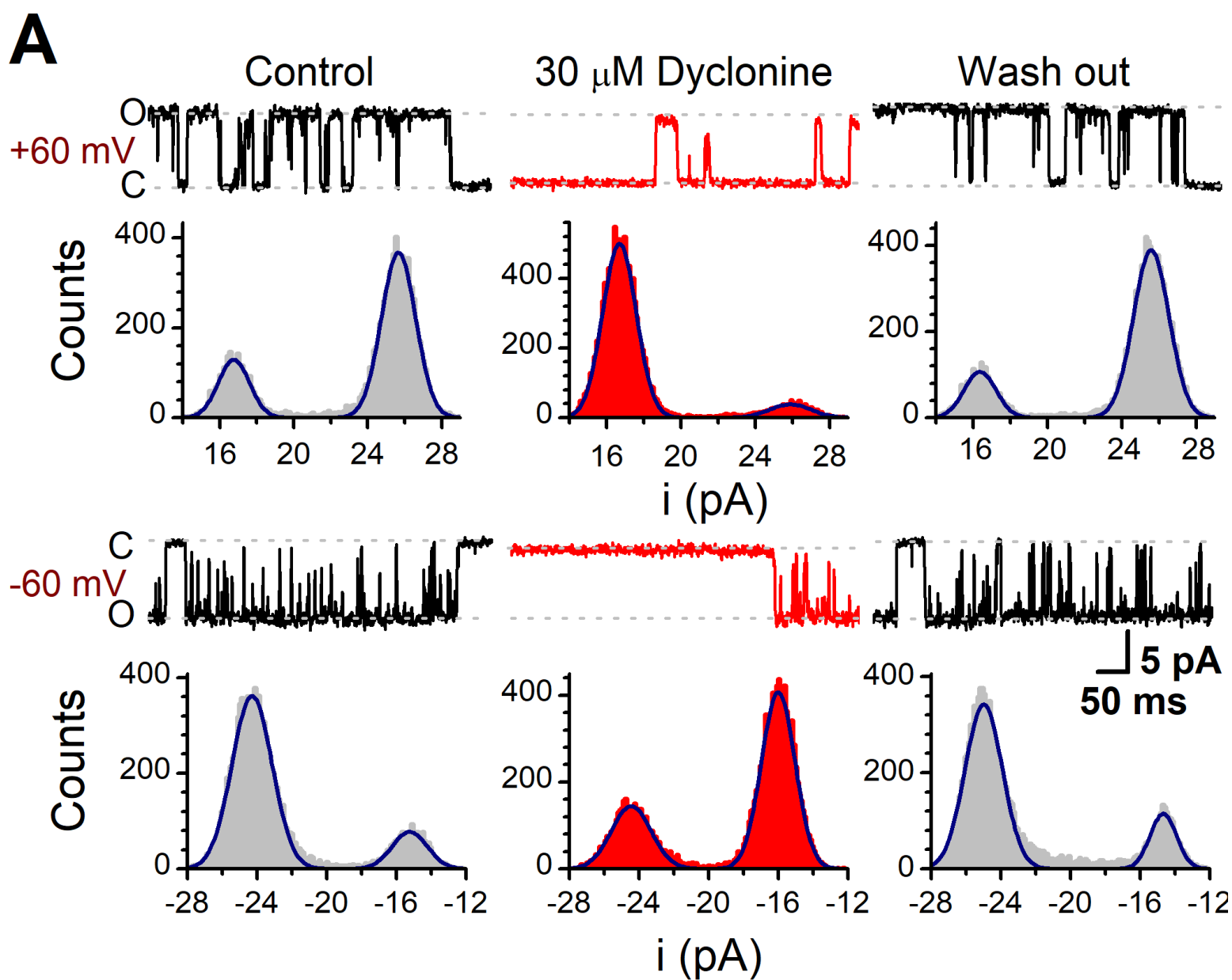


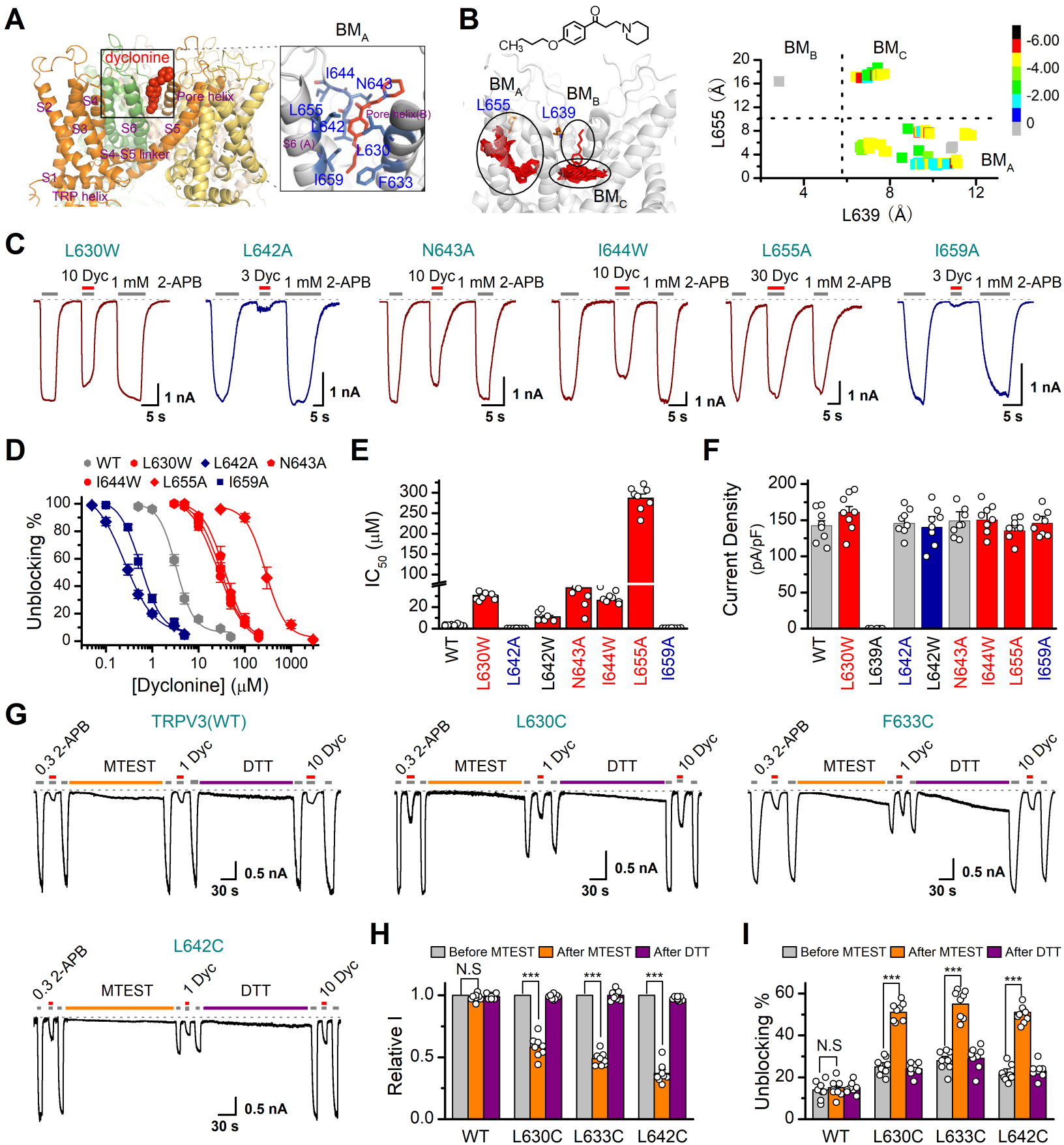


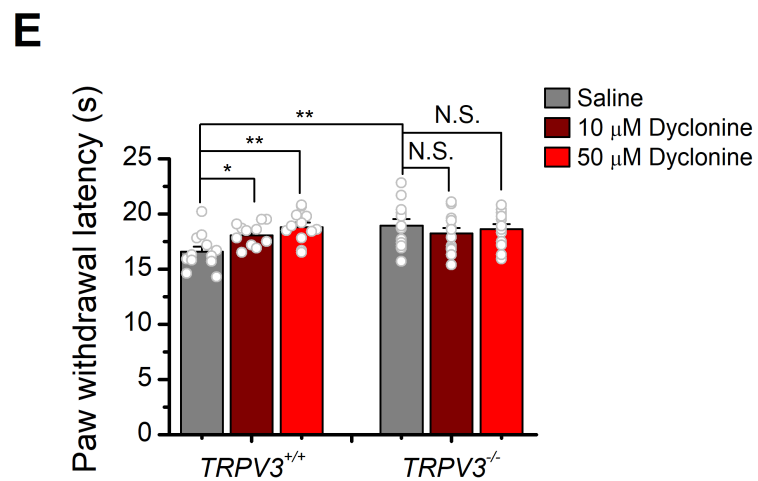
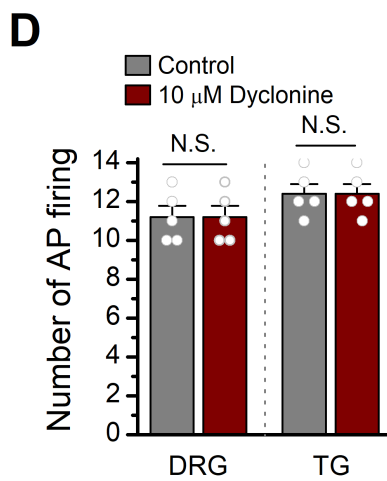
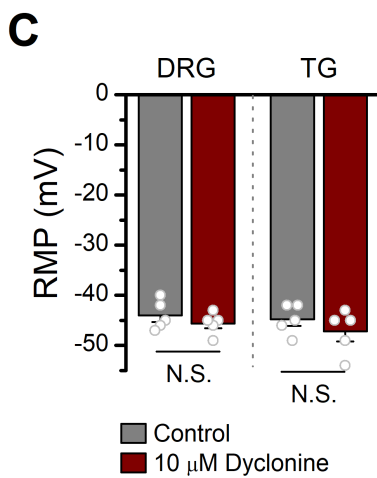
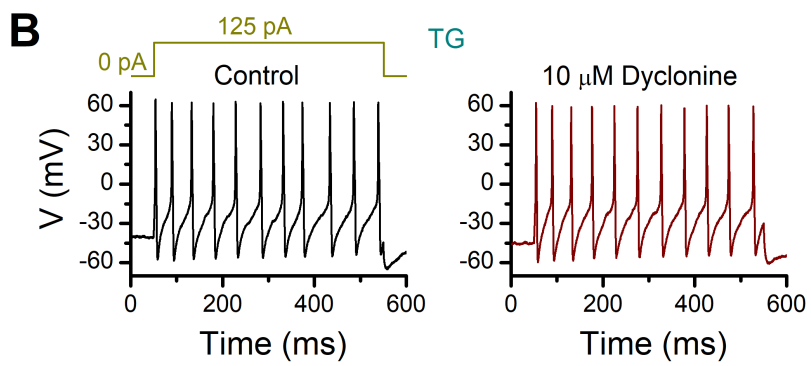
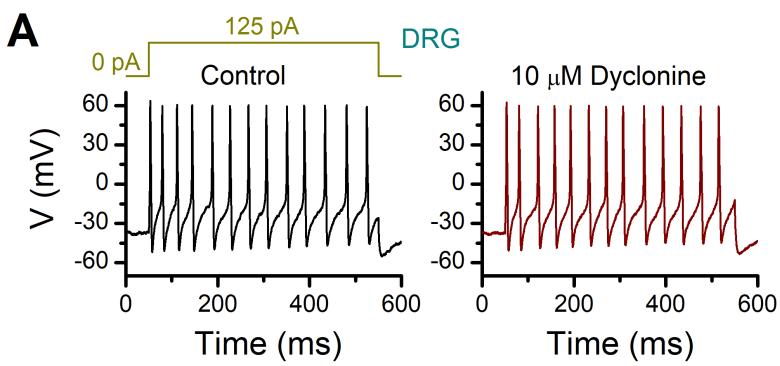


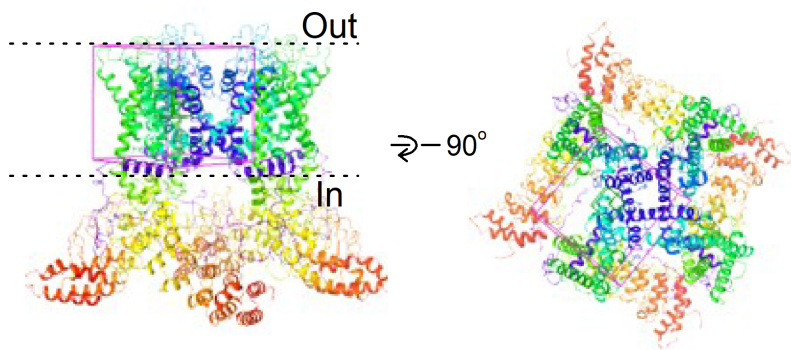
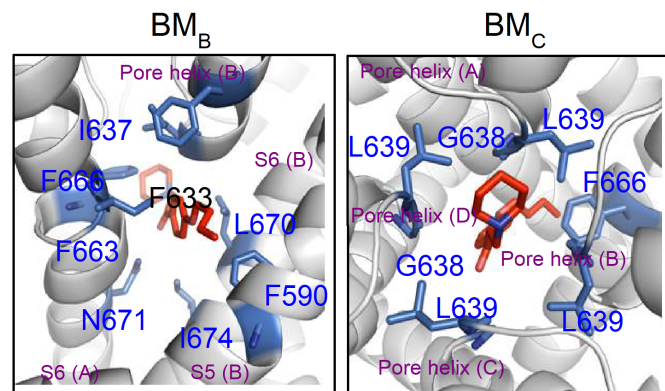
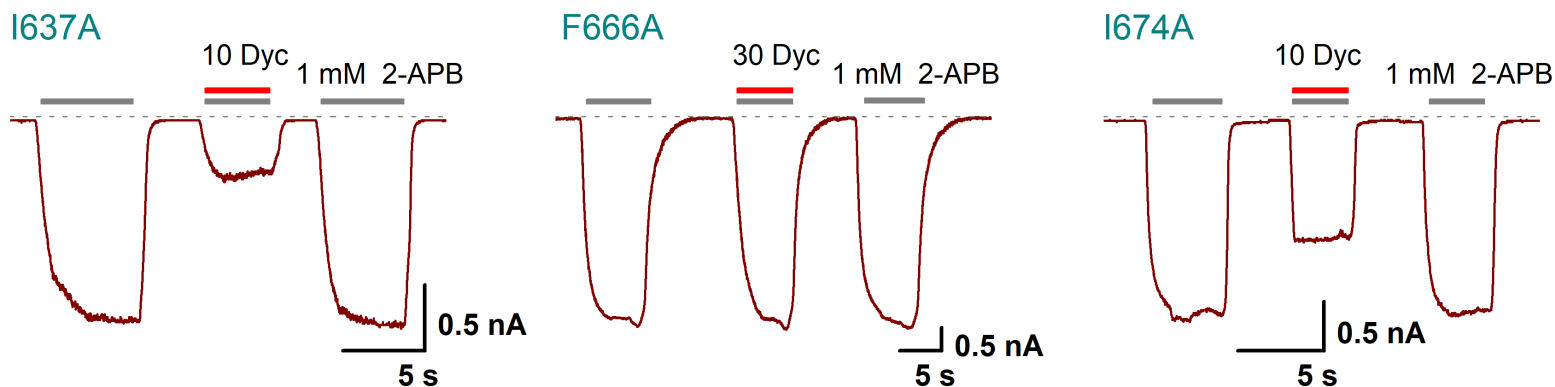
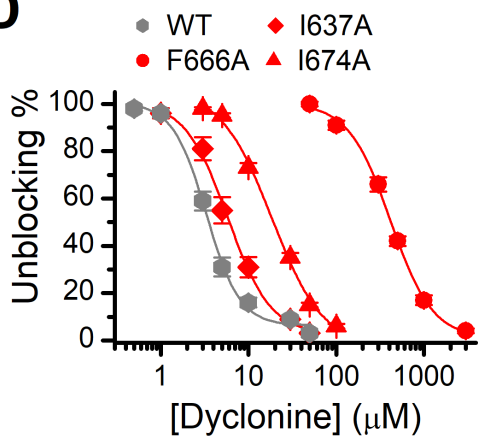
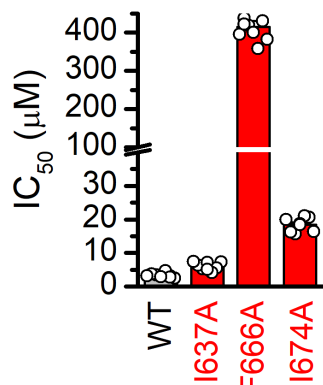
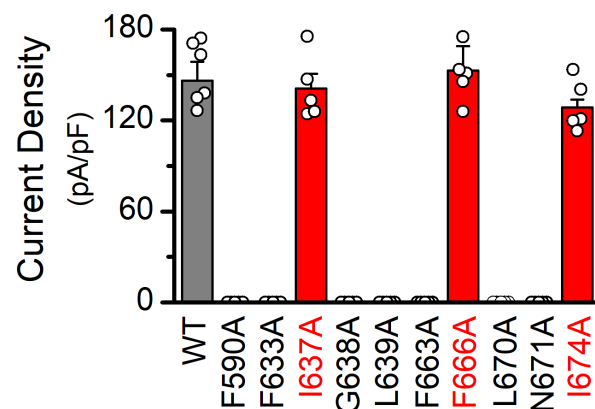
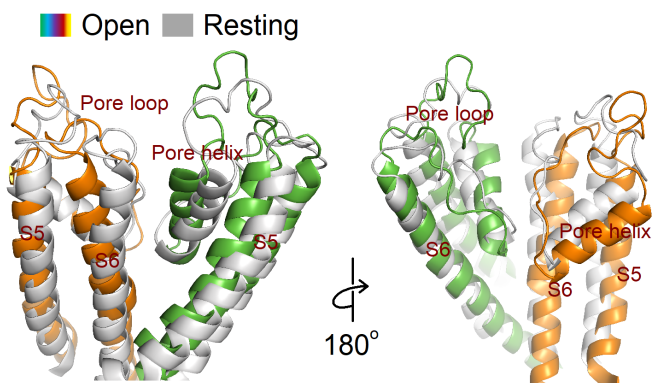










A**B****C****D****E****F****G****H**